

# SoxC and MmpReg promote blastema formation in whole-body regeneration of fragmenting potworms *Enchytraeus japonensis*

Received: 3 October 2022

Accepted: 22 July 2024

Published online: 22 August 2024

Toshiyuki Fujita<sup>1</sup>, Naoya Aoki<sup>1</sup> , Chihiro Mori<sup>2</sup>, Koichi J. Homma<sup>2</sup> & Shinji Yamaguchi<sup>1</sup>  

Regeneration in many animals involves the formation of a blastema, which differentiates and organizes into the appropriate missing body parts. Although the mechanisms underlying blastema formation are often fundamental to regeneration biology, information on the cellular and molecular basis of blastema formation remains limited. Here, we focus on a fragmenting potworm (*Enchytraeus japonensis*), which can regenerate its whole body from small fragments. We find *soxC* and *mmpReg* as upregulated genes in the blastema. RNAi of *soxC* and *mmpReg* reduce the number of blastema cells, indicating that *soxC* and *mmpReg* promote blastema formation. Expression analyses show that *soxC*-expressing cells appear to gradually accumulate in blastema and constitute a large part of the blastema. Additionally, similar expression dynamics of SoxC orthologue genes in frog (*Xenopus laevis*) are found in the regeneration blastema of tadpole tail. Our findings provide insights into the cellular and molecular mechanisms underlying blastema formation across species.

Regeneration is a prominent feature in many animals<sup>1</sup>. The degree of restoration of missing body parts or organs varies across species<sup>1–3</sup>. In highly regenerative animals, regeneration involves the formation of a blastema, which includes an undifferentiated mass of proliferative cells and provides the source material for lost body parts<sup>1,2,4–8</sup>. Hence, the mechanisms underlying blastema formation are fundamental for regeneration.

In vertebrates, the popular model systems for studying blastema formation are limb regeneration in salamanders and tail fin regeneration in zebrafish<sup>9</sup>. After wound healing, studies using lineage-tracing tools have identified that the connective tissue progenitors migrate to the amputation site and form regeneration blastema in both these model systems<sup>10,11</sup>. Among invertebrates, the highly regenerative animals are broadly distributed in many groups, including

Platyhelminths<sup>12</sup>, Annelids<sup>13</sup>, Xenacoelomorphs<sup>14</sup>, Cnidarians<sup>15</sup>, and Sponges<sup>16</sup>. Among them, some animals can regenerate whole bodies from small fragments of tissues<sup>7</sup>. Planaria is the most intensively studied model for whole-body regeneration, which includes blastema formation<sup>12</sup>. Several studies on regeneration in planaria have indicated that cell migration is crucial for blastema formation in invertebrates<sup>17–20</sup>. To clarify whether the cellular mechanisms underlying blastema formation can be generalized among broad animal species, they need to be verified in other model systems.

Annelids have long been used as model animals for studying regeneration because of their impressive regenerative abilities<sup>4,13,21,22</sup>. Some annelids exhibit regenerative abilities comparable to planaria, which can regenerate the entire body from small fragments<sup>7,13</sup>. In oligochaetes (a group of annelids that includes earthworms), a

<sup>1</sup>Department of Biological Sciences, Faculty of Pharmaceutical Sciences, Teikyo University, 2-11-1 Kaga, Itabashi-ku, Tokyo, Japan. <sup>2</sup>Department of Molecular Biology, Faculty of Pharmaceutical Sciences, Teikyo University, 2-11-1 Kaga, Itabashi-ku, Tokyo, Japan. ✉ e-mail: [shinji-y@pharm.teikyo-u.ac.jp](mailto:shinji-y@pharm.teikyo-u.ac.jp)

population of cells was speculated to migrate to blastema along the ventral nerve cord (VNC) from a distant location<sup>22–24</sup>, which has not yet been determined. Putative multipotent stem cells, called neoblasts in oligochaetes (in contrast, in planaria, neoblasts were shown to be multipotent by an elegant transplantation experiment<sup>25</sup>), are thought to be involved in this cell migration<sup>4</sup>; however, no solid evidence has been reported to date.

Three hypotheses have been put forth to explain oligochaete regeneration, and these theories have been believed for approximately 130 years despite the absence of definitive evidence: 1) the existence of multipotent neoblasts, 2) cell migration to the amputation site to form blastema, and 3) migration of cells to the blastema along the VNC<sup>4,13,22,24,26,27</sup>. Nevertheless, the germ cell precursor population has been reported to accumulate along the VNC towards the anterior blastema<sup>28</sup>. To date, some progress has been made in identifying the molecules involved in blastema formation in oligochaete<sup>29–33</sup>. However, these hypotheses are yet to be clearly addressed.

The potworm *Enchytraeus japonensis* Nakamura, 1993<sup>34</sup> is an enchytraeid (an oligochaete) reported in Japan. It reproduces asexually by dividing its body into several fragments, which then regenerate into complete individuals within 4–5 days<sup>34</sup> (Fig. 1a). The amputated fragments can similarly regenerate into whole bodies<sup>35</sup>. *Enchytraeus japonensis* is a small whitish animal that is approximately 10 mm in length and is easy to culture and handle. Additionally, blastema formation in *E. japonensis* is completed in approximately 24 h postamputation (hpa)<sup>36</sup>. All these features make *E. japonensis* an excellent laboratory animal for studying molecular and cellular basis underlying blastema formation.

In this work, using large-scale RNA-sequencing (RNA-seq) and the newly established functional RNA interference (RNAi) system in *E. japonensis*, we try to understand the molecular and cellular basis underlying blastema formation. We find *soxC* and *mmpReg* as upregulated genes in the blastema. RNAi of *soxC* and *mmpReg* reduce the number of blastema cells, indicating that *soxC* and *mmpReg* promote blastema formation. Expression analyses show that *soxC*-expressing cells appear to gradually accumulate in blastema and constitute a large part of the blastema. Furthermore, to examine whether the findings obtained using *E. japonensis* can be generalized across species, we conduct a comparative study using a tail regeneration model of a frog (*Xenopus laevis*) tadpole. We show similarity in the expression dynamics of SoxC genes in the blastema formation in *E. japonensis* and *X. laevis*, raising the possibility of common cellular mechanisms underlying blastema formation in both species.

## Results

### *soxC* is upregulated in blastema formation in *E. japonensis*

To understand the cellular and molecular basis of blastema formation in *E. japonensis*, we tried to identify the genes that were selectively expressed in the blastema. To this end, we explored the differentially expressed genes between blastema and other body parts in *E. japonensis* using RNA-seq. We devised a dose-dependent strategy to overcome the challenges associated with the surgical isolation of blastema. We increased the amount of blastema obtained by cutting the worms into multiple fragments. These fragments were sorted into two groups of blastema-containing fragments: worms cut into 3 fragments (blastema-poor group) and worms cut into 8 fragments (blastema-rich group). Additionally, the third group contained intact worms (Fig. 1b). In *E. japonensis*, blastema formation is completed in approximately 24 hpa<sup>36</sup>. We thus cut and cultured the worms for 24 h and used them for RNA-seq analysis (Fig. 1b). We generated a large-scale RNA-seq data and de novo assembled it to generate 291,660 contigs with NS0 value of 534 base pairs from all reads derived from the three libraries: blastema-rich group, blastema-poor group, and intact group. Among the 291,660 contigs, 86,094 common non-redundant contigs were detected in all three libraries (Fig. 1b). We

identified 1177 differentially expressed contigs between the blastema-poor and intact groups (Fig. 1c left and d) and 1593 differentially expressed contigs between the blastema-rich and intact groups (Fig. 1c right and d). We found 465 annotated genes that were differentially expressed (Fig. 1d). Among these, we identified 278 genes that were more upregulated in the blastema-rich group than in the blastema-poor group at 10 fragments per kilobase of exon per million reads mapped (FPKM) values or higher (Fig. 1c, d, Supplementary Data 1). Among 465 annotated genes, we found 398 genes in the blastema-poor group shared with blastema-rich group at 10 FPKM values or higher. We identified 124 genes that were more downregulated in the blastema-rich group than in the blastema-poor group at 10 FPKM values or higher (Supplementary Fig. 1a, Supplementary Data 2).

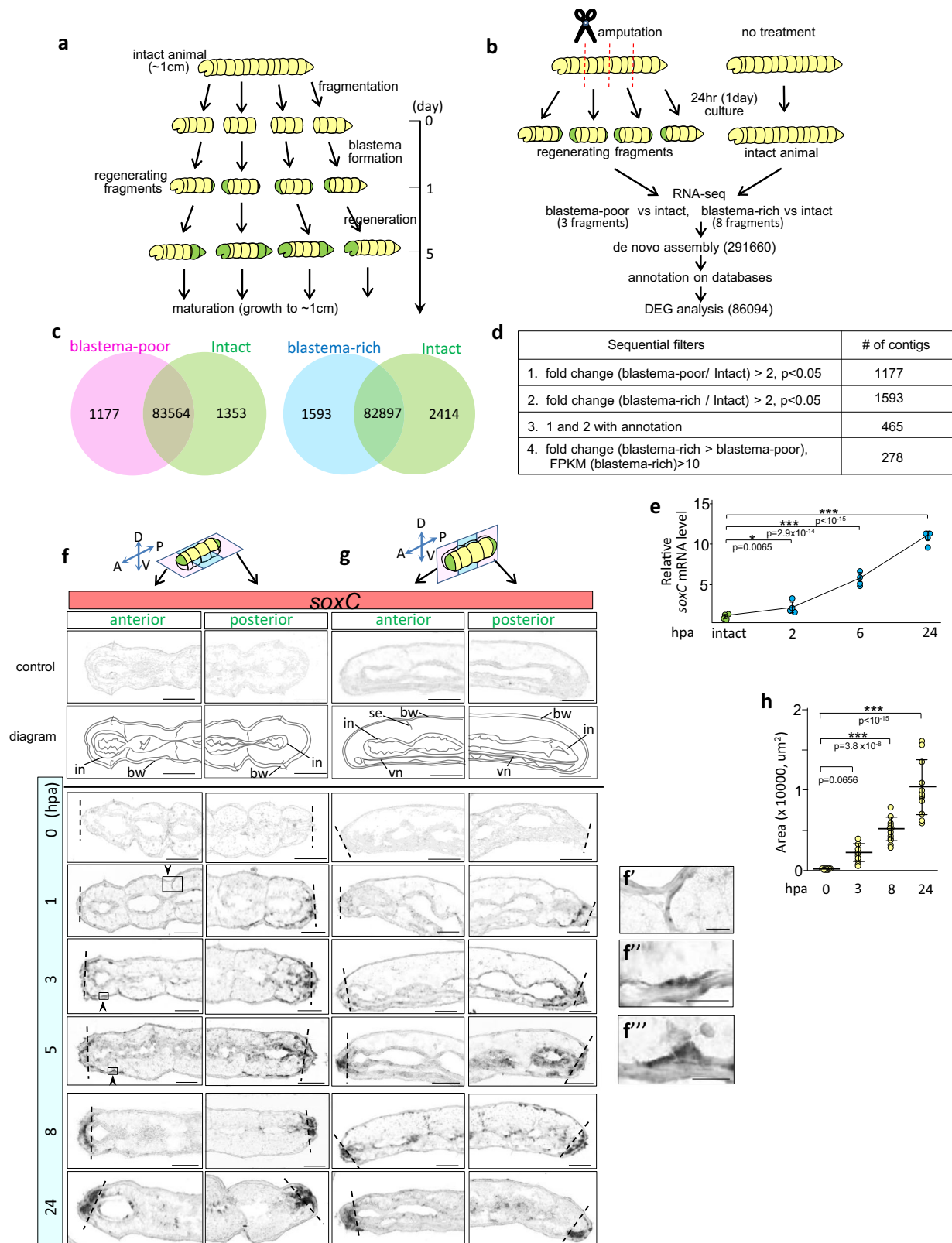
Among the 278 upregulated genes, we performed in situ hybridization (ISH) using 4 genes (*soxC*, *mmpReg*, *lrp8*, *nas36*) and found that all 4 were expressed in the blastema (*lrp8*, *nas36*; Supplementary Fig. 2a, b), suggesting that our strategy to identify genes associated with blastema was successful.

As transcription factors that act early in regeneration often establish and maintain cell identities<sup>37</sup>, we focused on transcription factors (Supplementary Data 3) among the 278 genes. The most upregulated gene among the transcription factors (7.9-fold upregulation in the blastema-rich group, Supplementary Data 3) belonged to the Sry-related high-mobility group (HMG) box (SOX)C transcription factor family. It contains a highly conserved HMG box DNA-binding domain (Supplementary Fig. 1b, c), which is distinct from other families, namely, SOXB and SOXD (Supplementary Fig. 1d). We named the gene *Ej-soxC* (hereafter referred to as *soxC*). As the SOX transcription factor family generally contributes to determining cell fate and identity in many lineages<sup>38</sup>, we further analyzed *soxC* by performing expression analysis using quantitative reverse-transcription polymerase chain reaction (qRT-PCR). We found that *soxC* was upregulated during blastema formation until 24 hpa (Fig. 1e) and leveled off at later stages (Supplementary Fig. 1e). This suggests that *soxC* is involved in the regeneration of *E. japonensis*, especially blastema formation.

To understand the role of *soxC* in blastema formation, we first examined the *soxC* expression pattern using ISH in horizontal and sagittal sections of the regenerating fragments (Fig. 1f, g). We did not detect *soxC*-positive cells just after amputation (0 hpa) and rarely detected them in intact worms (Supplementary Fig. 3), showing that *soxC* is not highly expressed in the homeostatic state. *soxC*-expressing cells were found close to the body wall and septa only near the posterior amputation site at 1 hpa (Fig. 1f, f'). At 3 hpa, *soxC*-expressing cells were found close to the body wall near both the anterior and posterior amputation sites (Fig. 1f, f', g). At 5, 8, and 24 hpa, we detected the *soxC*-expressing cells at both anterior and posterior amputation sites (Fig. 1f, f'', g). The area of *soxC*-expressing cells in the amputation site increased during blastema formation (Fig. 1h). At 24 hpa, the area of *soxC*-expressing cells encompassed a large part of the developing blastema (Fig. 1f, g, Supplementary Fig. 4a, b). The *soxC*-expressing cells observed close to the body wall (at 3 and 5 hpa) were spread out and flat (Fig. 1f', f''). Phalloidin staining showed that the shape of the cells close to the body wall were also spread out and flat at 5 hpa (Supplementary Fig. 4c–e). These shapes are typical of that of migrating cells<sup>39,40</sup>.

### *soxC* promotes blastema formation

To test whether *soxC* regulates blastema formation, we silenced *soxC* using RNAi by soaking or feeding the worms with double-stranded RNA (dsRNA) (Fig. 2a, b, Supplementary Fig. 4f). The *soxC* transcript level reduced by 40% (24 hpa) after soaking and feeding RNAi (Fig. 2c, Supplementary Fig. 4g). Interference efficiency was approximately the same in both methods. However, soaking RNAi takes less time than feeding RNAi; therefore, subsequent RNAi experiments were performed using the soaking RNAi method. *soxC* silencing significantly



decreased the number of cells around the amputation site compared with that of the control at 6 hpa (anterior: by 29%,  $p = 0.0127$ ; posterior: by 38%,  $p = 6.65 \times 10^{-5}$ ; Fig. 2d–g) and 24 hpa (anterior: by 33%,  $4.2 \times 10^{-4}$ ; posterior: by 27%,  $p = 0.00571$ ; Fig. 2h–k). As mentioned earlier, as the area of *soxC*-expressing cells encompassed a large part of the developing blastema (Fig. 1f, g, Supplementary Fig. 4a, b), we analyzed the size of blastema by visualizing *soxC* expression. *soxC* RNAi

decreased the volume of the blastema compared with that in the control at 6 hpa (by 59%,  $p = 5.6 \times 10^{-10}$ ) and 24 hpa (by 52%,  $p = 7.4 \times 10^{-8}$ ) (Fig. 2l–o). These data showed that *soxC* is required for functions in blastema formation. At 2 days post amputation (dpa), *soxC* RNAi-treated animals did not show a significant decrease in the number of cells in the blastema (Supplementary Fig. 5a–e). At 4 dpa, *soxC* RNAi-treated animals did not show significant difference in blastema

**Fig. 1 | *soxC* expression and blastema formation.** **a** *Enchytraeus japonensis* grows to about 10 mm in length and reproduces asexually by fragmentation approximately every 2 weeks. **b** Workflow of transcriptomic analyses during regeneration. Intact worms were amputated into 3 fragments (blastema-poor group) or 8 fragments (blastema-rich group). **c** Venn diagrams depicting selectively upregulated contigs in regenerating animals (blastema-poor and blastema-rich groups) compared with that of intact animals. **d** Sequential filters to select upregulated contigs in regenerating worms. We selected the genes that showed higher upregulation in the blastema-rich than in the blastema-poor group based on the FPKM value ( $>10$ ). **e** Expression level of *soxC* during regeneration. *soxC* was upregulated at 2, 6, and 24 hpa.  $n = 5$  for intact animals and for each time point. Error bars indicate the standard error of the mean (S.E.M.). **f, g** *soxC* expression during blastema formation at

0, 1, 3, 5, 8, and 24 hpa in horizontal sections (**f**) and sagittal sections (**g**). The sense controls and their diagrams are shown at the top. in, intestine; bw, body wall; se, septa; vn, ventral nerve cord. Dashed lines indicate amputation sites. **f** **f'** **f''** Magnified view of the boxed areas in (**f**) (1 hpa, arrowhead (**f'**); 3 hpa, arrowhead (**f''**); 5 hpa, arrowhead (**f'''**)). **h** Quantification of *soxC*-expressing areas in the anterior blastema of regenerating worms at 0 hpa ( $n = 11$ ), 3 hpa ( $n = 10$ ), 8 hpa ( $n = 12$ ) and 24 hpa ( $n = 12$ ). Data was combined from three independent experiments. The central lines and the error bars indicate the mean and standard deviation (SD), respectively.  $*p < 0.05$ ,  $**p < 0.01$ ,  $***p < 0.001$  (Dunnett's test) (**e, h**). Scale bars represent 100  $\mu\text{m}$  (**f, g**) and 20  $\mu\text{m}$  (**f', f'', f'''**). Source data are provided as a Source Data file. A: anterior, P: posterior, D: dorsal, V: ventral (**f, g**).

size, morphology, or the anti-acetylated tubulin antibody-labelled central and peripheral nervous system compared with that in the control RNAi-treated animals (Supplementary Fig. 5j–l). Proliferating cells were detected in the blastema of *soxC* RNAi- and control RNAi-treated animals (Supplementary Fig. 5m). These data suggested that *soxC* silencing did not affect regeneration at 2 and 4 dpa. Taken together, *soxC* is required for functions in blastema formation for at least up to 24 hpa, indicating that *soxC* promotes blastema formation.

### *mmpReg* promotes blastema formation

To further delineate the molecular basis of blastema formation in *E. japonensis*, we performed a Kyoto Encyclopedia of Genes and Genomes (KEGG) pathway analysis<sup>41</sup>. We mapped the 465 differentially expressed genes between regenerating and intact animals to functional categories (Fig. 3a). Among the 465 genes, we mapped 110 and frequently detected the extracellular matrix (ECM)-receptor interaction pathway category (Fig. 3b). This pathway analysis raised the possibility that ECM remodeling might modulate blastema formation. The cleavage of ECM components is one of the main processes during ECM remodeling<sup>42</sup>. We focused on matrix metalloprotease (MMP) because MMPs are the primary enzymes involved in ECM degradation<sup>42</sup>. Among the 278 genes that showed higher upregulation in the blastema-rich group than in the blastema-poor group, we found that only one gene encoded a protein belonging to the MMP family of extracellular proteases (35.8-fold upregulated in the blastema-rich group, Fig. 1d, Supplementary Fig. 6a and Supplementary Data 1). It was characterized by a pro-domain and a zinc-binding motif with potential catalytic properties and hemopexin-like motifs (Fig. 3c). Phylogenetic analysis showed that this *mmp* was somehow close to Japanese scallop *Mizuhopecten yessoensis* *MMP2-like* and sea mussels *Mytilus edulis* *MMP-17* (Supplementary Fig. 6b). qRT-PCR analysis showed that this *mmp* was upregulated during blastema formation until 24 hpa (Fig. 3d) and leveled off from 1 to 4 dpa (Supplementary Fig. 6c). This result suggests that this *mmp* may be involved in regeneration in *E. japonensis*, particularly in blastema formation. ISH showed that this *mmp* was expressed in the blastema at 5, 8, and 24 hpa (Fig. 3e, f) and in the chloragocytes, which are specialized peritoneal cells of unknown function (Supplementary Fig. 6d). These results also suggested that this *mmp* might be involved in blastema formation in *E. japonensis*.

To determine whether this *mmp* regulates blastema formation, we examined whether silencing this *mmp* using RNAi affected blastema formation. Soaking worms in this *mmp*-specific dsRNA reduced *mmp* expression by 40% at 24 hpa (Fig. 4a), which significantly decreased the number of cells around the amputation site compared with that in the control at 6 hpa (anterior: by 41%,  $p = 0.00109$ ; posterior: by 38%,  $p = 2.06 \times 10^{-4}$ ; Fig. 4b–e) and 24 hpa (anterior: by 40%,  $p = 9.1 \times 10^{-5}$ ; posterior: by 37%,  $p = 0.00165$ ; Fig. 4f–i). We analyzed blastema size by visualizing *soxC* expression. The *mmp* RNAi decreased blastema volume compared with that in control at 6 hpa (by 32%,  $p = 4.8 \times 10^{-6}$ ) and 24 hpa (by 38%,  $p = 2.7 \times 10^{-4}$ ) (Fig. 4j–m). Similarly, treatment with an MMP inhibitor (MMP2/MMP9 inhibitor I, N-([1,1'-biphenyl]-4-ylsulfonyl)-D-phenylalanine) decreased blastema volume (by 40%,

$p = 1.4 \times 10^{-5}$ ) (Fig. 4n,o). These data showed this *mmp* is required for functions in blastema formation. Therefore, we named this *mmp* *Ej-mmpReg* (Reg referring to regeneration, hereafter referred to as *mmpReg*). Similar to that of *soxC* RNAi-induced phenotype at 2 dpa, *mmpReg* RNAi-treated animals did not show a significant decrease in the number of blastema cells (Supplementary Fig. 5a, f–i). At 4 dpa, no significant difference was found in blastema size, morphology, or the nervous system (Supplementary Fig. 5j, n, o). Proliferating cells were detected in the blastema of *mmpReg* RNAi- and control RNAi-treated animals (Supplementary Fig. 5p). These data suggested that *mmpReg* silencing did not affect regeneration on 2 and 4 dpa. Taken together, *mmpReg* is required for functions in blastema formation for at least up to 24 hpa, indicating that *mmpReg* promotes blastema formation.

A limitation of our study is that the RNAi-induced phenotypes for *soxC* and *mmpReg* appeared to be relatively mild. Whether this phenomenon reflects gene function or the technical limits of our gene silencing system (e.g., quick recovery from RNAi-induced silencing by 2 dpa) is unclear. In our normal protocol, intact worms were soaked with dsRNA for 24 h and amputated worms were allowed to undergo regeneration on filter paper kept moist with Milli-Q water. To continuously treat amputated worms with dsRNA, we cultured them on filter paper kept moist with dsRNA solution until 2 dpa. At 2 dpa, animals continuously treated with *soxC* and *mmpReg* dsRNA did not exhibit a significantly reduced cell number in the blastema (Supplementary Fig. 5q–u), suggesting a similar phenotype to those treated following our normal protocol (Supplementary Fig. 5a–l, q–u).

### Cell proliferation and blastema formation

To clarify the mechanisms underlying *soxC* and *mmpReg* promoted blastema formation, we analyzed cell proliferation, which is a hallmark of blastema formation<sup>1</sup>. We investigated the cellular proliferation dynamics in the blastema using 5'-ethynyl-2'-deoxyuridine (EdU) labelling analysis to identify the time point at which the proliferating cells appeared in the blastema (Fig. 5a). The number of DAPI-labelled cells increased in the anterior (3 vs. 5 hpa,  $p < 0.05$ ; 3 vs. 8 hpa,  $p < 0.001$ ; 3 vs. 24 hpa,  $p < 0.001$ ; Fig. 5b, c, e) and posterior (3 vs. 5 hpa,  $p = 0.0634$ ; 3 vs. 8 hpa,  $p < 0.001$ ; 3 vs. 24 hpa,  $p < 0.001$ ; Fig. 5b, c, g) blastema regions, whereas the number of EdU-incorporated cells did not increase in the anterior (0–3 hpa vs. 3–5 hpa,  $p = 1$ ; 0–3 hpa vs. 5–8 hpa,  $p = 0.464$ ; Fig. 5b, d, f) and posterior (0–3 hpa vs. 3–5 hpa,  $p = 1$ ; 0–3 hpa vs. 5–8 hpa,  $p = 0.153$ ; Fig. 5b, d, h) blastema regions, but increased during 21–24 hpa in the blastema (vs. 0–3 hpa, anterior,  $p < 0.001$ ; posterior,  $p < 0.001$ ; Fig. 5b, d, f, h). These data showed that the number of cells increased, whereas that of proliferating cells rarely increased at 0–8 hpa. This suggests that the cells are supplied from elsewhere to the amputation site rather than proliferate at the amputation site up to 8 hpa.

Next, to explore whether *soxC* and *mmpReg* are required for functions in cell proliferation in the blastema, we examined the effect of *soxC* and *mmpReg* RNAi on cell proliferation (Fig. 6a, i). At 3 and 5 hpa, both *soxC* and *mmpReg* RNAi did not affect the number of anterior and posterior blastema cells (*soxC*,  $p > 0.05$  [Fig. 6b, c, e, g];



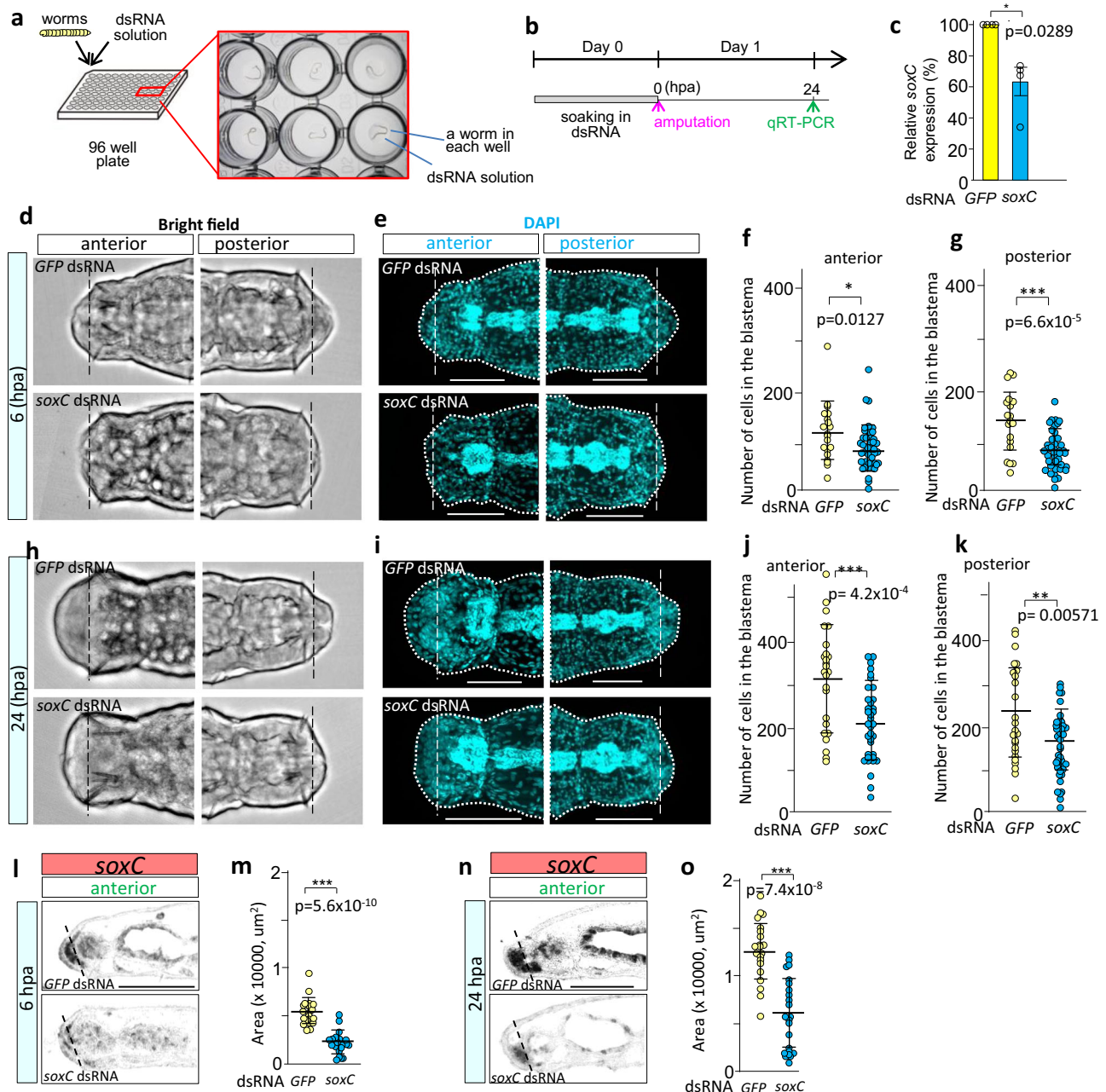


**Fig. 2 | *soxC* promotes blastema formation.** **a** Illustration of RNAi by soaking. **b** Schematic drawing of knock-down. Animals were amputated after 24 h of soaking in dsRNA and cultured for 1 day. **c** qPCR for the RNAi-mediated downregulation of *soxC* transcripts at 24 hpa ( $n = 4$ , biologically independent sample pools,  $p = 0.0289$ ). Error bars indicate S.E.M. **d, e** Representative images of RNAi animals at 6 hpa. Bright-field images (**d**). The nuclei were stained with DAPI (**e**). **f, g** RNAi of *soxC* reduced the number of cells in both the anterior blastema (*GFP* RNAi ( $n = 20$ ), *soxC* RNAi ( $n = 42$ ),  $p = 0.0127$ ) (**f**) and posterior blastema (*GFP* RNAi ( $n = 20$ ), *soxC* RNAi ( $n = 43$ ),  $p = 6.6 \times 10^{-5}$ ) (**g**). Representative of two independent experiments (**f, g**). **h, i** Representative images of RNAi animals at 24 hpa. Bright-field images (**h**). The nuclei were stained with DAPI (**i**). **j, k** RNAi of *soxC* reduced the number of cells in

both the anterior blastema (*GFP* RNAi ( $n = 25$ ), *soxC* RNAi ( $n = 36$ ),  $p = 4.2 \times 10^{-4}$ ) (**j**) and posterior blastema (*GFP* RNAi ( $n = 25$ ), *soxC* RNAi ( $n = 38$ ),  $p = 0.0057$ ) (**k**). Representative of two independent experiments (**j, k**). **l–o** *soxC* RNAi resulted in a decrease in the blastema volume at 6 hpa (*GFP* RNAi ( $n = 22$ ), *soxC* RNAi ( $n = 20$ ),  $p = 5.6 \times 10^{-10}$ ) (**m**) or 24 hpa (*GFP* RNAi ( $n = 21$ ), *soxC* RNAi ( $n = 23$ ),  $p = 7.8 \times 10^{-8}$ ) (**o**). Data was combined from two independent experiments (**m, o**). Typical images are shown (RNAi 6 hpa (**l**) or 24 hpa (**n**)). t-test, \* $p < 0.05$ , \*\* $p < 0.01$ , \*\*\* $p < 0.001$  (**c, f, g, j, k, m, o**). Error bars: mean  $\pm$  SD (**f, g, j, k, m, o**). Scale bars represent 250  $\mu$ m (**e, i, l, n**). Dashed lines indicate the position of amputation sites (**d, e, h, i, l, n**). Dotted lines indicate the outline of regenerating worms (**e, i**). Ventral views (**d, e, h, i**). Sagittal sections (**l, n**). Source data are provided as a Source Data file.

*mmpReg*,  $p > 0.05$  [Fig. 6j, k, m, o], except for *mmpReg* RNAi posterior at 5 hpa  $p = 0.0030$ ; Tukey–Kramer’s test) or proliferating cells (*soxC*,  $p > 0.05$  [Fig. 6b, d, f, h]; *mmpReg*,  $p > 0.05$  [Fig. 6j, l, n, p]; Tukey–Kramer’s test). At 8 hpa, *soxC* RNAi significantly decreased the number of cells around the amputation site compared with that in the control (anterior,  $p < 0.01$  [Fig. 6b, c, e]; posterior,  $p < 0.05$  [Fig. 6b, c, g]; Tukey–Kramer’s test), whereas the number of proliferating cells did

not significantly differ at 5–8 hpa in the blastema (anterior,  $p = 0.91$ , [Fig. 6b, d, f]; posterior,  $p = 0.33$ , [Fig. 6b, d, h]; Tukey–Kramer’s test). At 24 hpa, *soxC* RNAi reduced both the number of DAPI-stained cells (anterior,  $p < 0.01$ , [Fig. 6b, c, e]; posterior,  $p < 0.0001$ , [Fig. 6b, c, g]; Tukey–Kramer’s test) and EdU-incorporated proliferating cells (anterior,  $p < 0.001$ , [Fig. 6b, d, f]; posterior,  $p < 0.05$ , [Fig. 6b, d, h]; Tukey–Kramer’s test). Moreover, *mmpReg* RNAi elicited a similar effect

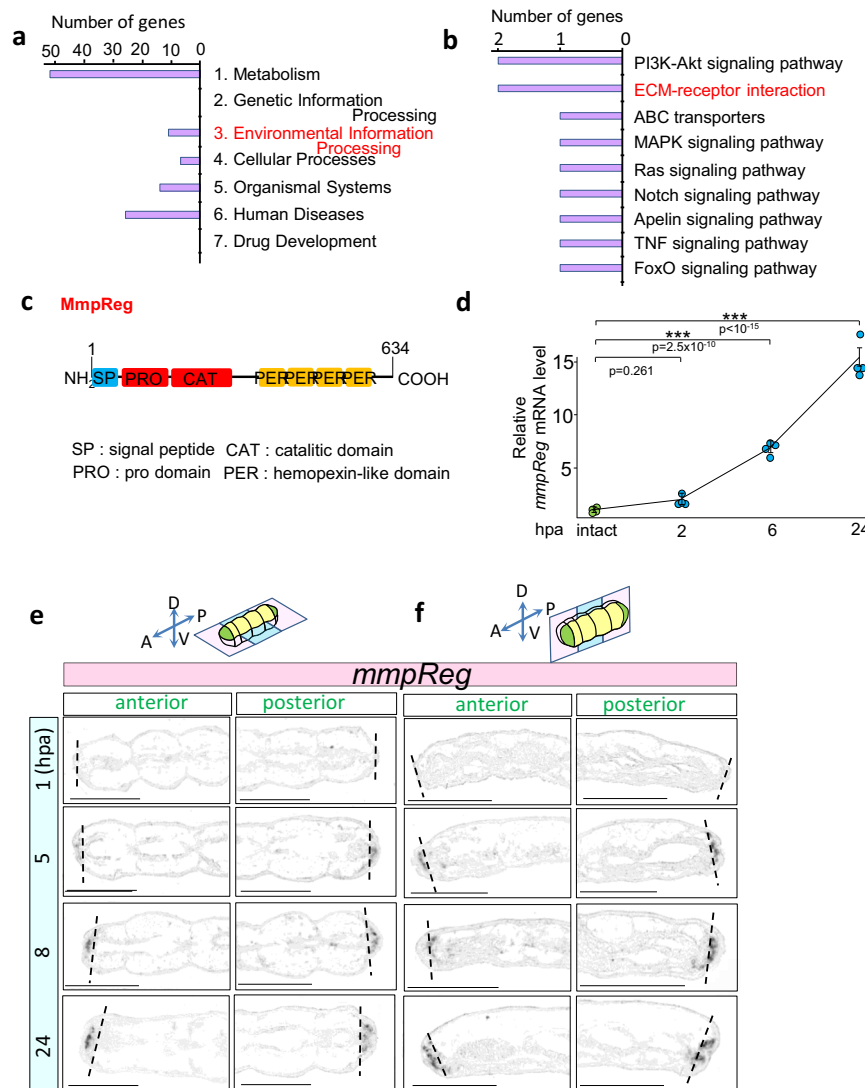


**Fig. 3 | *mmpReg* and blastema formation.** **a** KEGG pathway categories of frequently detected genes differentially expressed between regenerating and intact animals. **b** The KEGG pathway subcategories of frequently detected genes are categorized as environmental information processing in the upper panel. **c** Schematic of the predicted MmpReg structure of *E. japonensis*. **d** Expression level of *mmpReg* during regeneration. *mmpReg* was upregulated after 2, 6, and 24 hpa.

\*\*\* $p < 0.001$  (Dunnett's test). Error bars indicate S.E.M.  $n = 5$  for intact animals and for other time points. **e, f** *mmpReg* expression during blastema formation at 1, 5, 8, and 24 hpa using horizontal sections (**e**) and sagittal sections (**f**). Dashed lines indicate amputation sites. Scale bars represent 100  $\mu\text{m}$  (**e, f**). A: anterior, P: posterior, D: dorsal, V: ventral (**e, f**). Source data are provided as a Source Data file.

on the number of cells and cellular proliferation dynamics in blastema at 8 hpa (DAPI: anterior,  $p < 0.01$ ; posterior,  $p < 0.01$ , [Fig. 6j,k,m,o]; EdU: anterior,  $p = 0.57$ ; posterior,  $p = 0.44$ , [Fig. 6j, l, n, p]; Tukey-Kramer's test) and 24 hpa (DAPI: anterior,  $p < 0.0001$ ; posterior,  $p < 0.0001$ , [Fig. 6j, k, m, o]; EdU: anterior,  $p < 0.0001$ ; posterior,  $p < 0.01$ , [Fig. 6j, l, n, p]; Tukey-Kramer's test). These data showed that for at least up to 5–8 hpa, both *soxC* and *mmpReg* are not required for cell proliferation, but functions to supply cells to the amputation site; they are required subsequently for cell proliferation.

### Expression patterns of stem cell marker genes at homeostatic state

To elucidate the relationship between *soxC*-expressing cells and putative stem cells at the homeostatic state, we examined the expression patterns of known stem cell marker genes in *E. japonensis* (0 hpa or intact worm). We used the germline multipotency program (GMP) genes, including *piwi*, *vasa*, *nanos*, and *pl10*, as stem cell marker genes as they are broadly expressed in germline and multipotent stem cells in animals<sup>43</sup>. We analyzed the 86,094 assembled contigs obtained

from our transcriptomic analysis and identified two vasa genes (*Ej-vasa1* and *Ej-vasa2*), *Ej-nanos*, *Ej-pl10*, and *Ej-piwi* (Supplementary Fig. 8a,b,c). All five GMP genes were not differentially expressed between the blastema-rich and intact groups ( $>1.0$ - and  $<1.7$ -fold). The amino acid sequence of *Ej-vasa1* was similar to that of *Ej-vasa-like gene (vlg)-1* (89.9% identity, Supplementary Fig. 9a), and the amino acid sequence of *Ej-vasa2* was similar to that of *Ej-vlg-2* (86.6% identity, Supplementary Fig. 9b), as previously reported for *E. japonensis*<sup>44</sup>. Some previous studies have partially examined the expression patterns of some GMP genes in *E. japonensis*<sup>28,44,45</sup>. Our ISH analysis showed the presence of *Ej-vasa1*-positive cells close to the body wall just after amputation (0 hpa) (Fig. 7a, Supplementary Fig. 11a) and in intact worms (Supplementary Fig. 12a, b). The expression pattern of *Ej-vasa1* at 0 hpa was highly similar to those in intact worms, suggesting that 0 hpa time point can be considered as the homeostatic state. Consistent with a previous study<sup>28</sup>, *Ej-piwi*-expressing cells were found on the VNC (Fig. 7d). These cells act as germ cell precursors during gonad regeneration in *E. japonensis*<sup>28</sup>. *Ej-nanos* and *Ej-pl10* were expressed in the cells close to the body wall after amputation at 0 hpa

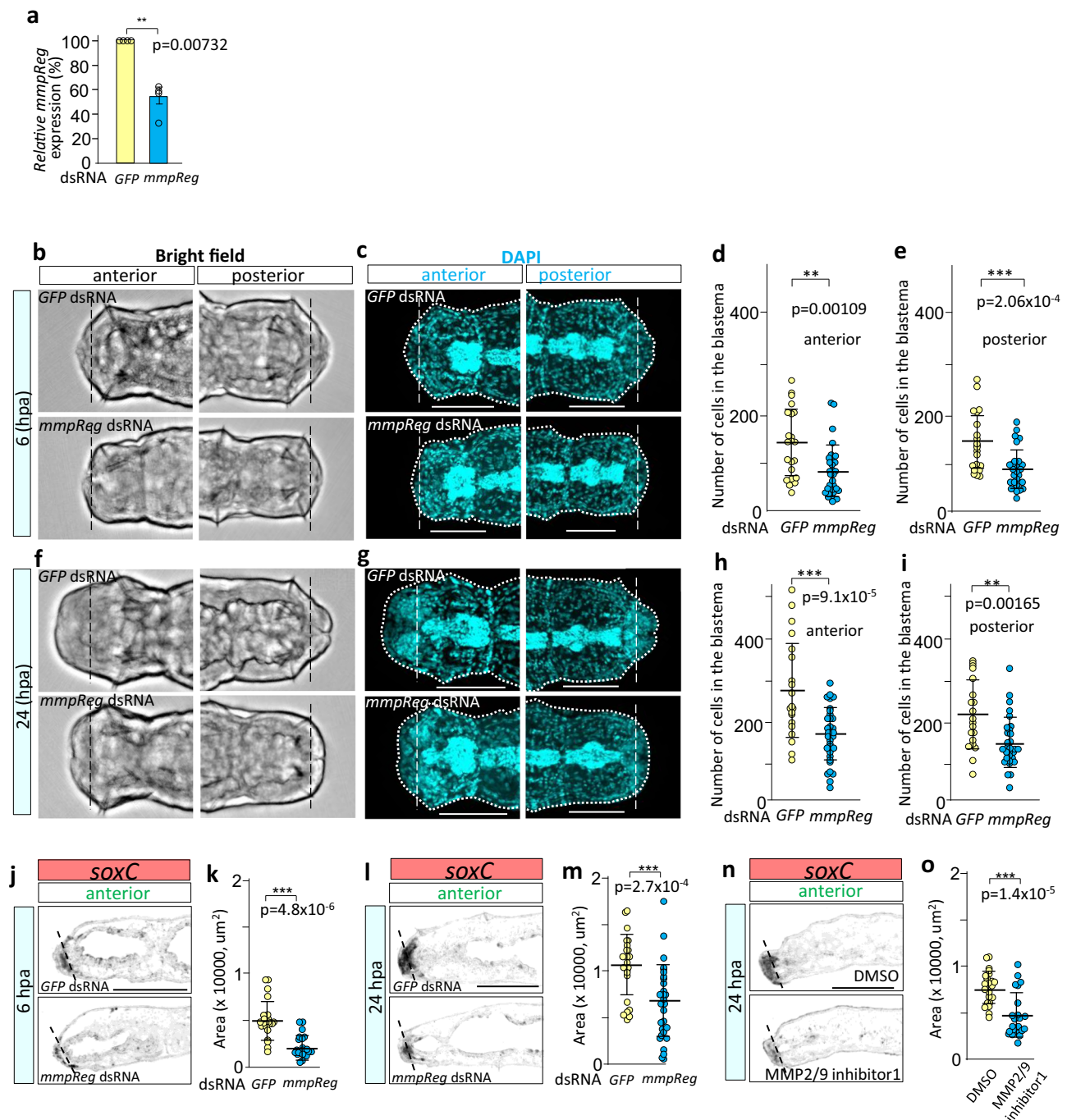


**Fig. 4 | *mmpReg* promotes blastema formation.** **a** qPCR for the RNAi-mediated downregulation of *mmpReg* transcripts at 24 hpa ( $n=4$ , biologically independent sample pools,  $p=0.00732$ ). Error bars indicate S.E.M. **b, c** Representative images of animals at 6 hpa. Bright-field images (**b**). The nuclei were stained with DAPI (**c**). **d, e** RNAi of *mmpReg* reduced the number of cells in both the anterior blastema (GFP RNAi ( $n=22$ ), *mmpReg* RNAi ( $n=30$ ),  $p=0.00109$ ) (**d**) and posterior blastema (GFP RNAi ( $n=22$ ), *mmpReg* RNAi ( $n=29$ ),  $p=2.06 \times 10^{-4}$ ) (**e**). Representative of two independent experiments (**d, e**). **f, g** Representative images of animals at 24 hpa. Bright-field images (**f**). The nuclei were stained with DAPI (**g**). **h, i** RNAi of *mmpReg* reduced the number of cells in the anterior blastema (GFP RNAi ( $n=20$ ), *mmpReg* RNAi ( $n=32$ ),  $p=9.1 \times 10^{-5}$ ) (**h**) and posterior blastema (GFP RNAi ( $n=20$ ), *mmpReg* RNAi ( $n=31$ ),  $p=0.00165$ ) (**i**). Representative of two independent experiments

(**h, i**). **j–m** *mmpReg* RNAi resulted in a decrease in the blastema volume at 6 hpa (GFP RNAi ( $n=22$ ), *mmpReg* RNAi ( $n=20$ ),  $p=4.8 \times 10^{-6}$ ) (**k**) or 24 hpa (GFP RNAi ( $n=24$ ), *mmpReg* RNAi ( $n=29$ ),  $p=2.7 \times 10^{-4}$ ) (**m**). Representative images are shown (RNAi 6 hpa (**j**) or 24 hpa (**l**)). **n, o** MMP inhibitor (MMP2/MMP9 inhibitor I, N-([1,1'-biphenyl]-4-ylsulfonyl)-D-phenylalanine, CAS#:193807–58-8) resulted in decreased blastema volume at 24 hpa (DMSO ( $n=22$ ), inhibitor ( $n=24$ ),  $p=1.4 \times 10^{-5}$ ) (**o**). Representative images are shown (MMP inhibitor (**n**)). Data was combined from two independent experiments (**k, m, o**). t-test,  $^*p < 0.05$ ,  $^{**}p < 0.01$ ,  $^{***}p < 0.001$  (**a, d, e, h, i, k, m, o**). Error bars: mean  $\pm$  SD (**d, e, h, i, k, m, o**). Scale bars represent 250  $\mu\text{m}$  (**c, g, j, l, n**). Dashed lines indicate amputation sites (**b, c, f, g, j, l, n**). Dotted lines indicate the outline of regenerating worms (**c, g**). Ventral views (**b, c, f, g**). Sagittal sections (**j, l, n**). Source data are provided as a Source Data file.



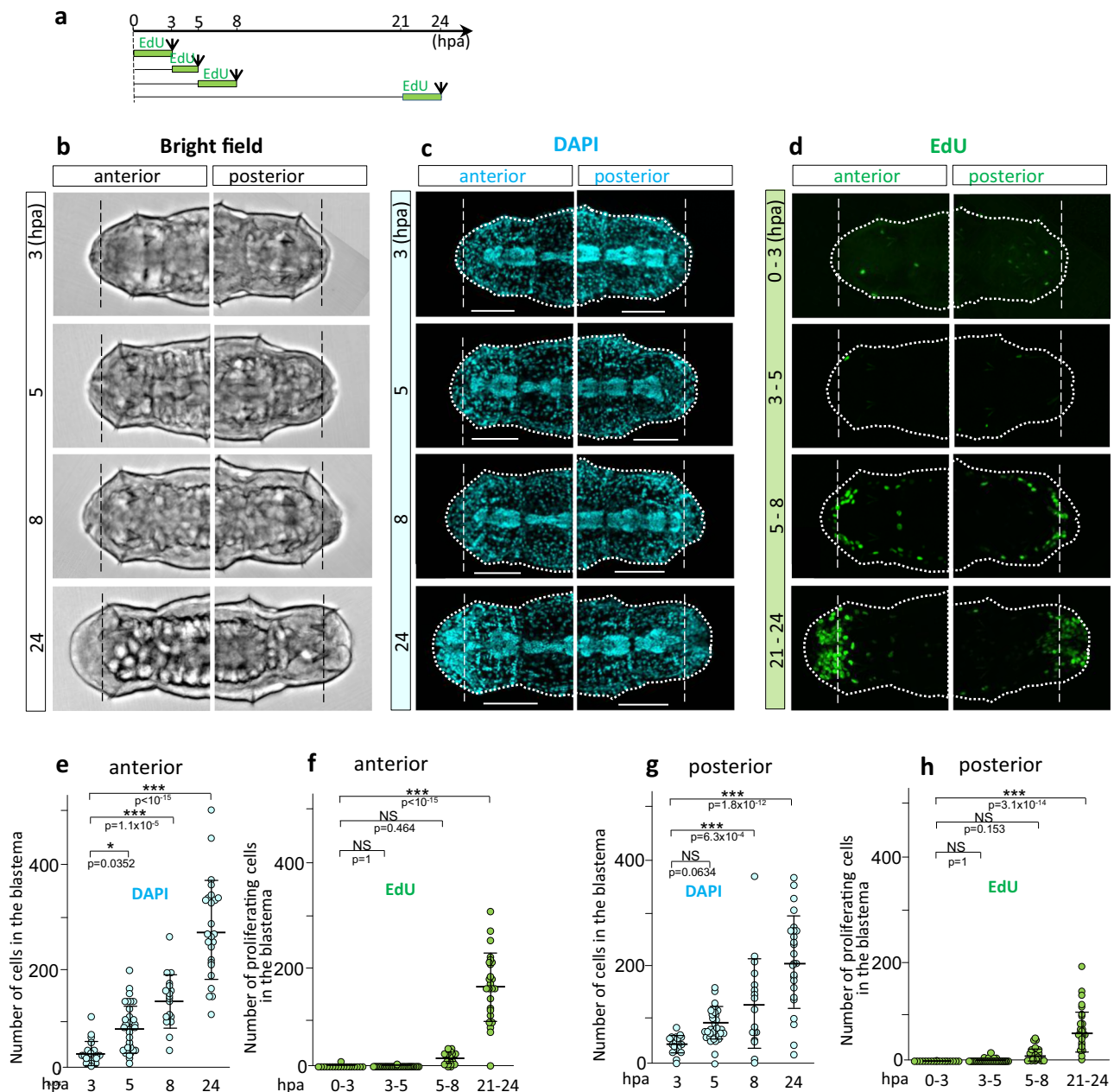


**Fig. 5 | Distribution of proliferating cells in blastema formation.** **a** Schematic drawing of EdU labelling. Small arrows indicate the fixation points with PFA-PBS. **b, c, d** Representative images of regenerating animals at 3, 5, 8 and 24 hpa. Bright-field images (**b**). The nuclei were stained with DAPI (**c**). EdU-incorporated cells (**d**). **e, f, g, h** The number of cells increased in both anterior blastema (**e**, 3 hpa ( $n = 18$ ), 5 hpa ( $n = 32$ ), 8 hpa ( $n = 18$ ), 24 hpa ( $n = 25$ )) and posterior blastema (**g**, 3 hpa ( $n = 19$ ), 5 hpa ( $n = 32$ ), 8 hpa ( $n = 18$ ), 24 hpa ( $n = 25$ )). The number of proliferating

cells did not significantly increase (0–3 vs 3–5, 0–3 vs 5–8 hpa), but increased at 21–24 hpa (0–3 vs 21–24 hpa) in anterior and posterior blastema (**d, f, h**).  $^*p < 0.05$ ,  $^{**}p < 0.01$ ,  $^{***}p < 0.001$ . NS indicates not significant (Dunnett's test). Representative of two independent experiments (**e, f, g, h**). Error bars: mean  $\pm$  SD (**e, f, g, h**). Scale bars represent 250  $\mu$ m (**c, g, j, l, n**). Dashed lines indicate amputation sites (**b, c, d**). Dotted lines indicate the outline of regenerating worms (**c, d**). Ventral views (**b, c, d**). Source data are provided as a Source Data file.

(Fig. 7b, c, Supplementary Fig. 11b, c) but *Ej-piwi* and *Ej-vasa2* were not detected in the cells close to the body wall after amputation at 0 hpa (Fig. 7d, e, Supplementary Fig. 11d, e). Additionally, *Ej-vasa2* was expressed in cells in the body cavity at 0 hpa (Fig. 7e). The expression patterns of all GMP genes that were tested differed from that of *soxC* in a homeostatic state.

Next, we examined the expression pattern of the GMP genes in the body parts where putative stem cells are considered to be present: the posterior growth zone (PGZ), gonad (recently referred to as multipotent progenitor cell (MPC) clusters in a marine annelid *Capitella teleta*<sup>46</sup>), and neoblasts<sup>13</sup>. The gonad expressed all GMP genes that were examined (*Ej-vasa1*, *Ej-vasa2*, *Ej-nanos*, *Ej-pl10*, *Ej-piwi*) (Fig. 7f),

whereas PGZ expressed all GMP genes except *Ej-piwi* (*Ej-vasa1*, *Ej-vasa2*, *Ej-nanos*, *Ej-pl10*) (Fig. 7f, Supplementary Fig. 11f). In contrast, the neoblasts only expressed *Ej-vasa1* (Fig. 7g, Supplementary Fig. 10). Furthermore, *soxC* was expressed in PGZ but not in the gonad and neoblasts (Supplementary Figs. 3a, b, 10b). Taken together, these data showed that the expression patterns of the tested GMP genes were different from that of *soxC* except for PGZ.

### Expression dynamics of *soxC* and GMP genes are different

To understand the relationship between *soxC*-expressing cells and putative stem cells during blastema formation, ISH for the GMP genes was performed. At 5 hpa, *soxC*-expressing cells were present



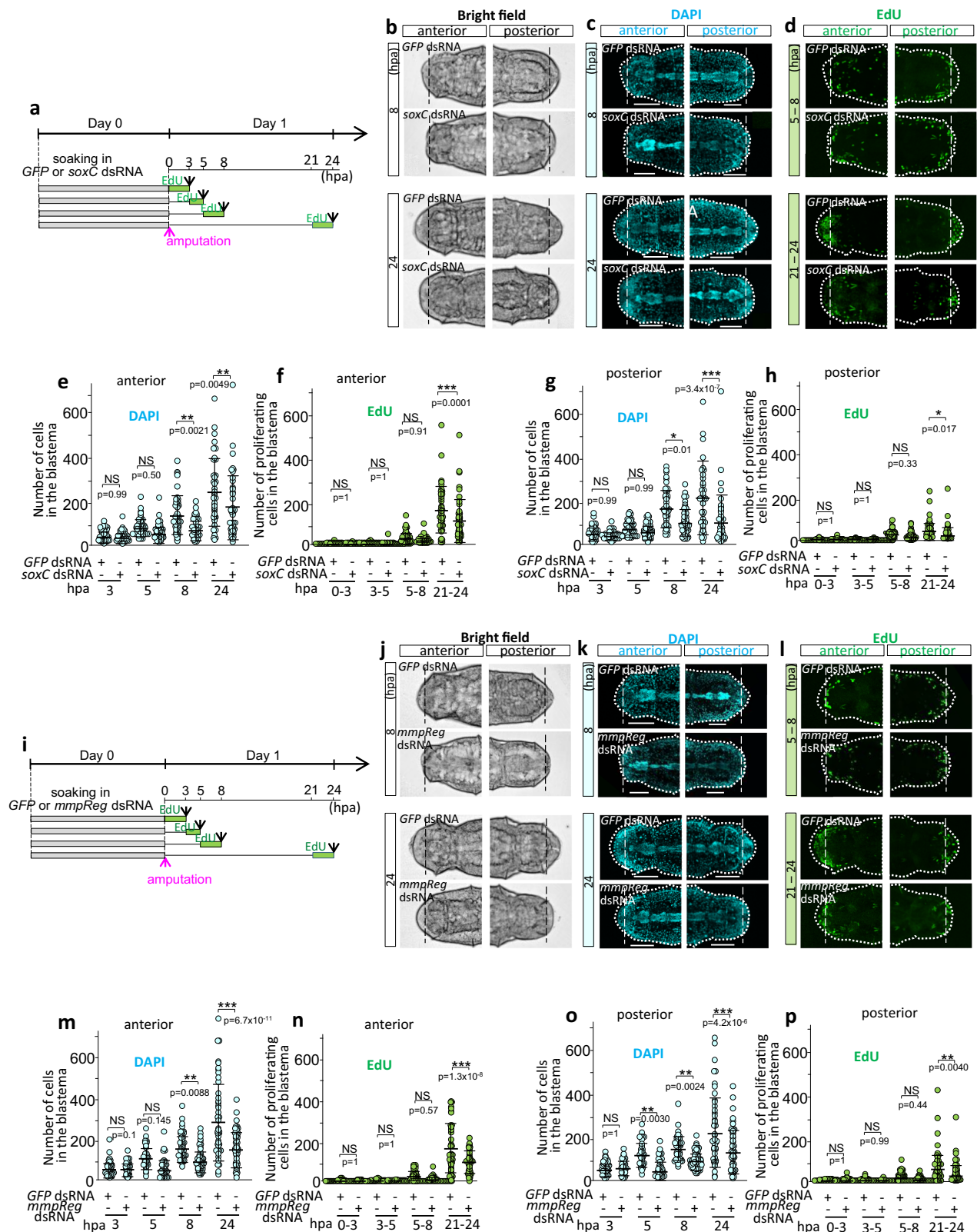


(Fig. 1f,g) but *Ej-vasa1*-expressing cells were absent in the blastema (Fig. 7a). In contrast, at 24 hpa, *Ej-vasa1* was expressed in a small portion of the blastema (Fig. 7a), which is reminiscent of the results of previous studies in other annelids<sup>47,48</sup> that GMP genes were expressed de novo in the early blastema. To clarify the relationship between the *Ej-vasa1*-expressing and *soxC*-expressing cells, we examined whether *Ej-vasa1* and *soxC* were co-expressed in blastema.

A double ISH analysis revealed that the *soxC* and *Ej-vasa1* expression patterns did not fully overlap in the blastema (18 out of 18 fragments) (Fig. 8). *Ej-piwi*-expressing cells were not found in the blastema even at 0–24 hpa (Fig. 7d). Similarly, *Ej-nanos*, *Ej-pl10*, and *Ej-vasa2* were not detected in the cells near the anterior or posterior amputation sites at 0–5 hpa (Fig. 7a, b, c, e) but were expressed in a small portion of the blastema at 24 hpa (Fig. 7a,b,c,e). The neoblasts

**Fig. 6 | Distribution of proliferating cells in the blastema of RNAi-subjected worms.** **a** Schematic drawing of EdU labelling in *soxC* RNAi-subjected worms. Small arrows indicate the fixation points with PFA–PBS. **b, c, d** Representative images of regenerating animals at 8 and 24 hpa. Bright-field images (**b**). The nuclei were stained with DAPI (**c**). EdU-incorporated cells (**d**). **e, f, g, h** Quantification of DAPI-stained cells. 3 hpa (*GFP* ( $n = 41$ ), *soxC* ( $n = 43$ )), 5 hpa (*GFP* ( $n = 47$ ), *soxC* ( $n = 44$ )), 8 hpa (*GFP* ( $n = 43$ ), *soxC* ( $n = 44$ )), 24 hpa (*GFP* ( $n = 40$ ), *soxC* ( $n = 42$ )) in the anterior blastema (**e**) and 3 hpa (*GFP* ( $n = 40$ ), *soxC* ( $n = 42$ )), 5 hpa (*GFP* ( $n = 46$ ), *soxC* ( $n = 41$ )), 8 hpa (*GFP* ( $n = 43$ )), *soxC* ( $n = 44$ )), 24 hpa (*GFP* ( $n = 38$ ), *soxC* ( $n = 38$ )) in the posterior blastema (**g**). Quantification of EdU-incorporated cells in the anterior blastema (**f**) and posterior blastema (**h**). **i** Schematic drawing of EdU labelling in *mmpReg* RNAi worms. Small arrows indicate the fixation points

with PFA–PBS. **j, k, l** Representative images of regenerating animals at 8 and 24 hpa. Bright-field images (**j**). The nuclei were stained with DAPI (**k**). EdU-incorporated cells (**l**). **m, n, o, p** Quantification of DAPI-stained cells. 3 hpa (*GFP* ( $n = 40$ ), *soxC* ( $n = 31$ )), 5 hpa (*GFP* ( $n = 35$ ), *soxC* ( $n = 34$ )), 8 hpa (*GFP* ( $n = 45$ ), *soxC* ( $n = 52$ )), 24 hpa (*GFP* ( $n = 44$ ), *soxC* ( $n = 44$ )) in the anterior blastema (**m**) and 3 hpa (*GFP* ( $n = 39$ ), *soxC* ( $n = 31$ )), 5 hpa (*GFP* ( $n = 35$ ), *soxC* ( $n = 34$ )), 8 hpa (*GFP* ( $n = 44$ )), *soxC* ( $n = 51$ )), 24 hpa (*GFP* ( $n = 43$ ), *soxC* ( $n = 44$ )) in the posterior blastema (**o**). Quantification of EdU-incorporated cells in the anterior blastema (**n**) and posterior blastema (**p**). \* $p < 0.05$ , \*\* $p < 0.01$ , \*\*\* $p < 0.001$ . NS indicates not significant (Tukey–Kramer's test). Error bars: mean  $\pm$  SD (**e, f, g, h, m, n, o, p**). Dashed lines indicate amputation sites (**b, c, d, j, k, l**). Dotted lines indicate the outline of regenerating worms (**c, d, k, l**). Ventral views (**b, c, d, j, k, l**). Source data are provided as a Source Data file.

only expressed *Ej-vasa1* at 0–24 hpa (Fig. 7g, Supplementary Fig. 10a). The expression pattern of all the tested GMP genes varied considerably from that of *soxC* during blastema formation, particularly at 0–5 hpa.

### Expression dynamics of *soxC* genes during tadpole tail blastema formation

We consider the possibility that animals other than annelid may display similar expression dynamics of *soxC* during blastema formation because SOXC transcription factors are widely conserved across animals<sup>49</sup>. In many vertebrates, SOX4, SOX11, and SOX12 constitute the SOXC family<sup>50</sup>. We examined this possibility using blastema in regenerating the African claw frog (*X. laevis*, amphibian) tadpole tail. Blastema formed within 48 hpa in the tadpole tail<sup>51</sup> (Fig. 9a). ISH was performed using serial sections of regenerating tadpole tail. It showed that *Xl-sox4* and *Xl-sox11* were not detected just after amputation at 0 hpa (Fig. 9b,e); only *Xl-sox11* was expressed around amputation sites at 6 hpa (Fig. 9b,e). Then, both *Xl-sox4* and *Xl-sox11* were expressed around amputation sites at 24 hpa (Fig. 9b,c), particularly underneath the outer layer that covers the wounds (Fig. 9c,f). At 48 hpa, *Xl-sox4* and *Xl-sox11* were expressed abundantly in the blastema (Fig. 9b,e). Time-course ISH analysis showed that *Xl-soxC*-expressing cells appeared to accumulate gradually in the blastema. qRT-PCR showed that the *Xl-sox4* and *Xl-sox11* expression levels increased in the regenerating tadpole tail, including the blastema (Fig. 9d,g). Overall, these data indicate that the regenerating frog tadpole tail displays similar expression dynamics as that of *soxC* in *E. japonensis* in blastema formation.

### Discussion

In this study, we identified 278 upregulated (Fig. 1d, Supplementary Data 1) and 124 downregulated (Supplementary Fig. 1a, Supplementary Data 2) genes involved in blastema formation in *E. japonensis* using large-scale RNA-seq. Additionally, we developed a system for silencing genes in the potworms, which involves soaking or feeding the worms with dsRNA. This system is an easily applicable, reproducible, and minimally invasive strategy for gene silencing (Figs. 2a–o, 4a–m, 6a–p, Supplementary Fig. 5a–p) (the first RNAi study using injection in *E. japonensis* was published by Takeo, et al.<sup>33</sup>). We expect that analyzing the functions of the genes on our lists using the functional RNAi tool would significantly contribute to enhancing our understanding of the molecular and cellular basis of blastema formation in *E. japonensis*. Here, we present the significance of two genes (*soxC* and *mmpReg*) that are upregulated in blastema formation.

We found that *soxC* was rarely expressed in the homeostatic state (Supplementary Fig. 3) and was upregulated during regeneration (Fig. 1f,g). After amputation, *soxC* was expressed selectively close to the body wall and septa near the amputation site at 1 hpa (posterior) and 3 hpa (anterior and posterior) (Fig. 1f,g). The *soxC*-expressing cells near the body wall were spread out and flat (Fig. 1f',f''), which is typical of migrating cells<sup>39,40</sup>. Subsequently, the area in which *soxC* was

expressed gradually increased (Fig. 1f,g). The area of *soxC*-expressing cells encompassed to a large part of the developing blastema at 24 hpa (Fig. 1f,g, Supplementary Fig. 4a,b). Furthermore, *soxC* silencing led to a significant decrease in the number of cells around the amputation site at 6 and 24 hpa (Fig. 2a–o), showing that *soxC* is required for functions in blastema formation at least up to 24 hpa. Taken together, these results suggest that *soxC* can be used as a representative marker for blastema formation (Fig. 10a).

The multipotent stem cells maintained in the adults (hereafter referred to as adult stem cells (ASCs)) of other whole-body regeneration animals generally express GMP genes<sup>7,52</sup>. For instance, neoblasts in planaria are molecularly defined by the expression of *piwi*-*I53*. Multipotent interstitial stem cells (i-cells) in *Hydra* expressed *piwi*, *Vasa*, and *PL10*<sup>54,55</sup>. We found that in *E. japonensis*, *Ej-vasa1* was expressed in all putative ASC niches, which we have described subsequently. Furthermore, *Ej-vasa1* was expressed abundantly in the homeostatic state (Supplementary Fig. 12a). These results suggest that *Ej-vasa1* can be used as a representative marker for ASCs in *E. japonensis*. Additionally, GMP genes were not found in blastema at 0–5 hpa (Fig. 7a–e). In contrast, *soxC* was not detected at 0 hpa (Fig. 1f,g) and was expressed in blastema at 3–5 hpa (Fig. 1f,g), showing that *soxC* and *Ej-vasa1* distribution patterns differed in blastema. Moreover, their distribution patterns did not fully overlap in blastema (Fig. 1f, g, Fig. 7a), as confirmed by the double ISH analysis results at 24 hpa (Fig. 8). Taken together, these data suggest that a part of the ASC population differed from that of the *soxC*-expressing cells. Currently, the relationship between *soxC*-expressing cells and ASCs remains unclear, and further information may be obtained by enumerating the relationship between *soxC*-expressing cells and ASCs in annelid blastema formation (Fig. 10a).

In annelids, putative ASCs found in the PGZ, gonad (recently referred to as MPC clusters in a marine annelid, *C. teleta*<sup>46</sup>), and neoblasts<sup>13</sup>. The PGZ of annelids is a highly proliferative region at the posterior tip of the body that produces new segments during normal growth<sup>48,56,57</sup>. In *E. japonensis*, the PGZ expressed all the tested GMP genes with the exception of *Ej-piwi*, showing that PGZ contains putative ASCs (Fig. 7f, Supplementary Fig. 11f). Additionally, *soxC* was expressed in the PGZ at the homeostatic state (Supplementary Figs. 3, 10b), suggesting that *soxC* is also involved in normal growth. The gonad was identified in the 7<sup>th</sup> and 8<sup>th</sup> segments in *E. japonensis*<sup>28</sup>. A pair of neoblasts are located adjacent to the septa in each *E. japonensis* segment<sup>58</sup>. Neoblasts of annelids have been hypothesized to correspond to ASCs<sup>4</sup>, although this is yet to be proven. In contrast, in planaria, neoblasts were proven to be multipotent through an elegant transplantation experiment<sup>25</sup>. In *E. japonensis*, neoblasts only expressed *Ej-vasa1* (Fig. 7g), whereas the cells close to the body wall expressed *Ej-vasa1*, *Ej-nanos*, and *Ej-pl10* (Fig. 7a–c). The GMP gene-expressing cells close to the body wall appeared to be distinct from neoblasts. These results suggest the heterogeneity of *vasa1*-expressing ASCs.

Historically, many studies have speculated that a population of cells might migrate to blastema along the VNC<sup>4,13,23,24</sup> instead of through the

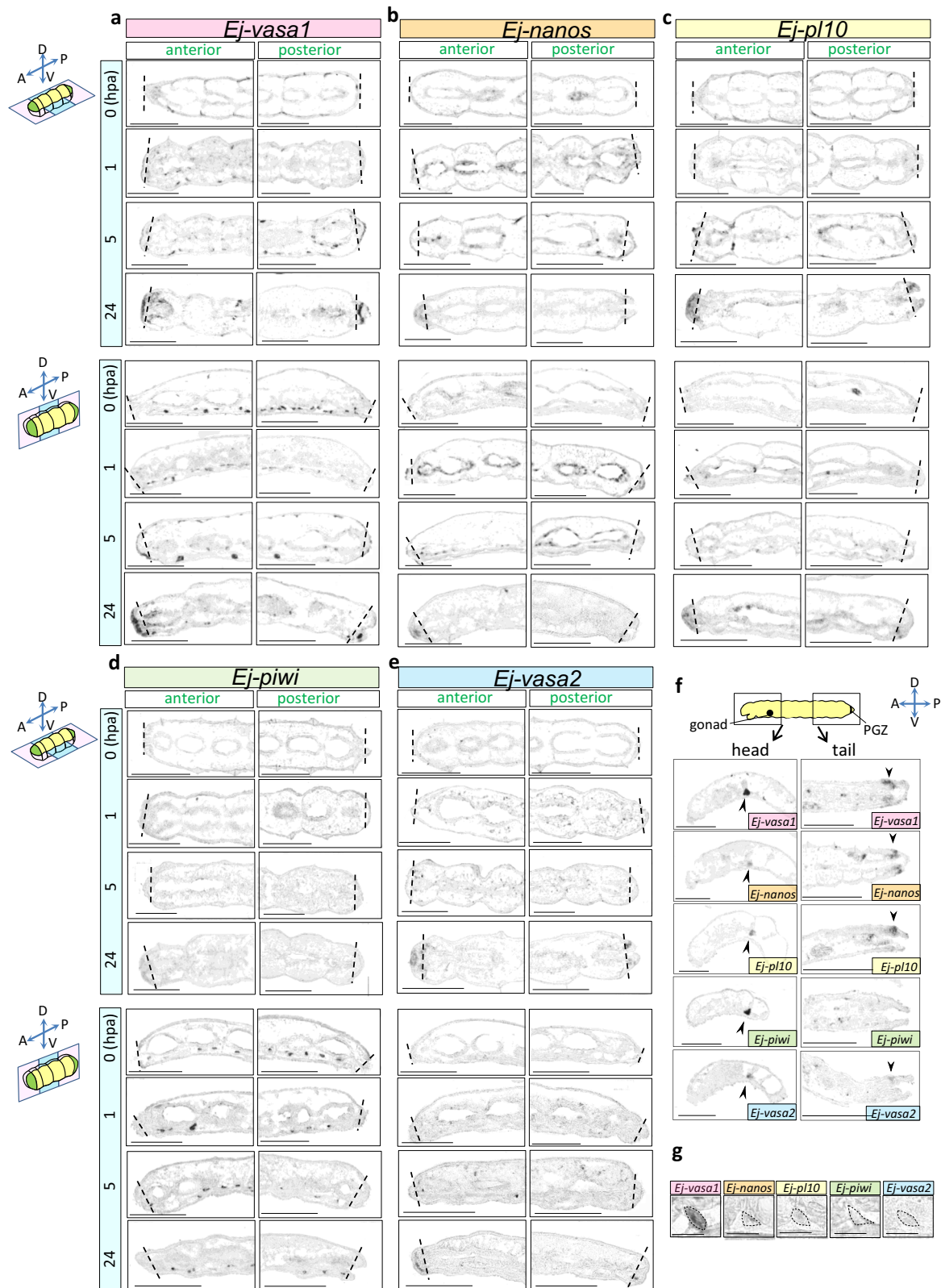


**Fig. 7 | Expression of GMP genes during blastema formation in *E. japonensis*.** **a–e** GMP gene (*Ej-vasa1* (a), *Ej-nanos* (b), *Ej-pl10* (c), *Ej-piwi* (d), *Ej-vasa2* (e)) expression during blastema formation at 0, 1, 5, and 24 hpa in horizontal sections (upper eight panels) and sagittal sections (lower eight panels). Dashed lines indicate amputation sites. **f** GMP gene expression in gonad and PGZ at 0 hpa. Expression level varies depending on the GMP gene, but all GMP genes were expressed in the gonad and PGZ, except for *Ej-piwi* in PGZ at 0 hpa. Arrowheads in the left panels

indicate the position of the gonad, and arrowheads in the right panels indicate the position of PGZ. **g** GMP gene expression in neoblast at 0 hpa. *Ej-vasa1* was expressed in neoblasts, whereas the other GMP genes were not detected in neoblasts at 0 hpa. The regions around the septa are shown in each panel. Dotted lines indicate the outline of neoblasts. Scale bars represent 250  $\mu$ m (a–f) and 20  $\mu$ m (g). A: anterior, P: posterior, D: dorsal, V: ventral (a–f). All images are representative of at least two independent experiments (a–g).



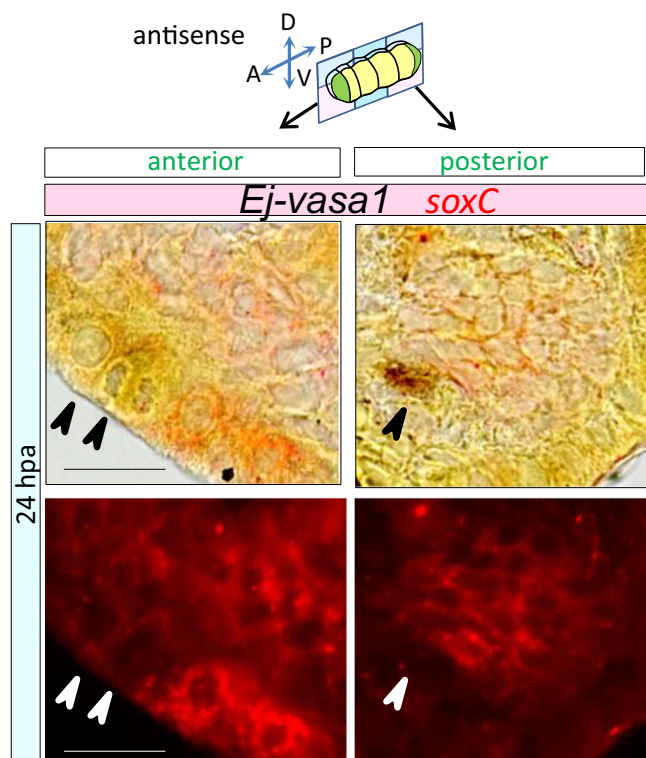


**Fig. 8 | Double ISH of *soxC* and *Ej-vasa1* in blastema formation.** DIG-labeled *soxC* and fluorescence-labeled *Ej-vasa1* RNA antisense probes were used for double ISH in horizontal sections of regenerating worms at 24 hpa. Arrowheads indicate the position of *Ej-vasa1*-expressing cells. Scale bars represent 25  $\mu$ m. Representative of two independent experiments.

body wall in oligochaete; however, limited evidence is available. Recently, time-lapse imaging of a freshwater annelid *Pristina leidyi* showed wound-directed migrating cells<sup>40</sup>. However, these migrating cells were detected and classified using purely morphological features, with no molecular markers available. Owing to the lack of molecular markers, the types of cells that contribute to blastema formation remain unknown. To date, ISH analysis in *E. japonensis* using GMP genes as markers has shown that *Ej-vasa1*-expressing cells and *Ej-piwi*-expressing cells are attached to the dorsal side of the VNC<sup>28,44</sup> (consistent with the data shown in Fig. 7a, d) and that *Ej-vasa1* and *Ej-piwi* are co-expressed<sup>44</sup>. *Ej-piwi*-expressing germ cell precursors attached to the VNC were suggested to migrate to blastema<sup>28</sup>. However, *Ej-piwi*-expressing cells were not detected in the blastema at 0–24 hpa<sup>28</sup> (consistent with our data in Fig. 7d). Hence, no evidence exists that *Ej-piwi*-expressing cells are related to blastema formation at least 0–24 hpa. Another study claimed that *Ej-vasa1*-expressing cells found close to the body wall could migrate to blastema based on the results of an ISH analysis at 48 hpa<sup>45</sup>. However, we found that *Ej-vasa1*-expressing cells were not detected in the blastema at 0–5 hpa (Fig. 7a), whereas a certain number of DAPI-stained cells were detected in blastema up to 5 hpa (Fig. 5c,e,g). Hence, no evidence exists that *Ej-vasa1*-expressing cells are related to blastema formation at least at 0–5 hpa. In contrast, *soxC*-expressing cells were found close to the body wall and septa near the amputation site at 1 hpa (posterior) and 3 hpa (anterior and posterior) (Fig. 1f,g). Time-course ISH analysis showed that *soxC*-expressing cells appeared to gradually accumulate in the blastema (Fig. 1f,g). The area of *soxC*-expressing cells encompassed to a large part of the developing blastema (Fig. 1f,g, Supplementary Fig. 4a,b). Expression dynamics of *soxC* tended to coincide with the increase in the number of DAPI-stained cells during blastema formation (Figs. 1h, 5e,g). Additionally, RNAi experiments showed that *soxC* is required for functions in blastema formation at 6 and 24 hpa (Fig. 2a–o). All these data

suggest that *soxC*-expressing cells contribute to blastema formation. We further investigated the cellular proliferation dynamics in the blastema using EdU labelling analysis and found that the number of cells in the blastema gradually increased before they started proliferating at 8 hpa (Fig. 5a–h). This suggests that the cells were supplied from elsewhere to the amputation site up to 8 hpa rather than proliferated. Before the onset of cell proliferation, *soxC* RNAi led to a significant decrease in the number of cells in blastema (Fig. 6a,b,c,e,g). This result suggests that *soxC* is required for functions to supply cells from elsewhere to the amputation site up to 8 hpa. Taken together, possibly, *soxC*-expressing cells may be the cells supplied to the amputation site (Fig. 10a).

We identified *mmpReg* as another upregulated gene in blastema formation. Recently, a single-cell RNA-seq (scRNA-seq) study in salamander limb regeneration showed that *Mmp8* and *Mmp13* were upregulated during blastema formation, indicating extensive ECM remodeling by MMPs<sup>59</sup>. Similar to the results obtained using *soxC* RNAi, *mmpReg* silencing decreased the number of cells in blastema and delayed blastema formation at 6 and 24 hpa. Before onset of cell proliferation (at 8 hpa), *mmpReg* RNAi significantly decreased the number of cells in the blastema (Fig. 6a,b,c,e,g). We analyzed the size of blastema by visualizing *soxC* expression. At 6 and 24 hpa, *mmpReg* RNAi and MMP inhibitor decreased the volume of the blastema (Fig. 4j–o). Our data indicate that *mmpReg* promotes blastema formation. Notably, the role of *MmpReg* in regenerating *E. japonensis* needs to be clarified by determining the substrate ECM proteins and the stimulation factors that release *MmpReg* to better understand the whole picture of blastema formation at the molecular level. Currently, we did not detect an epistatic relationship between *soxC* and *mmpReg* in terms of level of expression by knock-down (Supplementary Fig. 7a,b). However, further investigation of the relationship between *soxC*-expressing cells and *MmpReg* could provide valuable information.

SOXC transcription factors are widely conserved across animals<sup>49</sup>. SOX4 and SOX11 (in mammals, SOX4, SOX11, and SOX12 constitute the SOXC family) were highly expressed in embryonic epidermal cells and re-expressed in postnatal skin wounds in mice<sup>60</sup>. SOX4 and SOX11 regulate downstream cytoskeleton genes, one of which was required for cell migration<sup>60</sup>. In zebrafish, the result of a knock-down analysis suggested that *sox11b* regulates the migration of Muller glia-derived progenitor cells and their fate determination during retina regeneration<sup>61</sup>. During cerebral development in mice, Sox11 inhibition suppressed the radial migration of cortical neurons<sup>62</sup>. Overall, these results in addition to those inferred from the present study suggest that SOXC gene(s)-expression may be a characteristic of migrating cells across different contexts and animal species.

If SOXC gene(s)-expression reflects a characteristic of blastema cell mass across different animal species, similar expression dynamics in blastema formation would be found in other animals. We found *Xl-sox4* and *Xl-sox11*-expressing cells appeared to accumulate in the blastema in the regenerating tadpole tail. Our data point to a similarity in the expression dynamics of SoxC genes in the blastema formation in *E. japonensis* and *X. laevis*, raising the possibility of common cellular mechanisms underlying blastema formation in both species (Fig. 10b). Recently, in the cnidarian polyp *Hydra vulgaris*, *HuSoxC* was found to be expressed in a transition state between i-cells and differentiated cells, which suggests that *HuSoxC* is a marker for cells in a transition state<sup>63</sup>. At present, whether *HuSoxC*-expressing cells migrate is unknown, and further studies are warranted to determine the migration capabilities of the *HuSoxC*-expressing cells. In planaria, scRNA-seq suggested that *soxP-1* is expressed in multiple lineage progenitors<sup>64</sup>. In the acol worm *Hofstenia miamia*, scRNA-seq suggested that *sox-1* was expressed in the likely neural specialized neoblast population<sup>65</sup>. However, the relationship of *soxP-1* in planaria or *sox-1* in acol worm and SOXC family needs to be verified. Notably, examining the expression dynamics of *soxP-1* in planaria and *sox-1* in acol worm in blastema formation may provide important information. Further



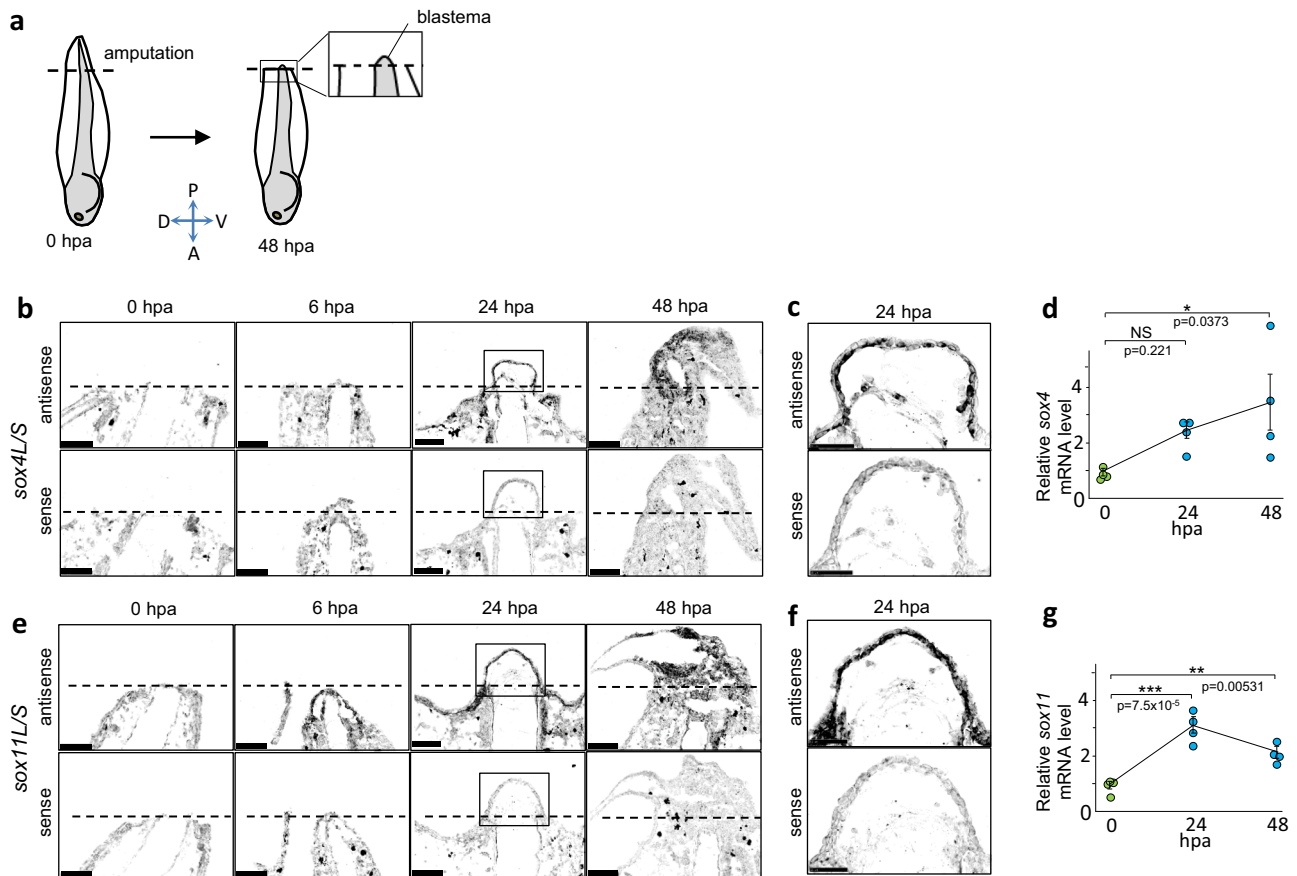


**Fig. 9** | *Xl-sox4* and *Xl-sox11* expression in the blastema formation of tadpole tails. **a** Schematic drawing of tadpole tail blastema formation. A: anterior, P: posterior, D: dorsal, V: ventral. **b** *Xl-sox4* expression during blastema formation at 0, 6, 24 and 48 hpa. The sense controls are shown on the lower panels. **c** Magnified view of the boxed areas in **(b, 24 hpa)**. **d** Expression level of *Xl-sox4* during blastema formation. *sox4* was upregulated after amputation.  $n = 4$  for time points. **e** *Xl-sox11*

expression during blastema formation at 0, 6, 24 and 48 hpa. The sense controls are shown on the lower panels. **f** Magnified view of the boxed areas in **(e, 24 hpa)**. **g** Expression level of *Xl-sox11* during blastema formation. *Xl-sox11* was upregulated after amputation.  $n = 4$  for time points. **(d, g)** Error bars indicate S.E.M. \* $p < 0.05$ , \*\* $p < 0.01$ , \*\*\* $p < 0.001$  (Dunnett's test). Dashed lines indicate amputation sites **(a, b, e)**. Source data are provided as a Source Data file.

studies on the expression dynamics and behavior of *SOXC* gene(s)-expressing cells in various regeneration animal models would help understand whether the cellular mechanisms underlying blastema formation can be generalized among across species.

## Methods

### Animals

*Enchytraeus japonensis*<sup>34</sup> worms were reared in 1.0% agar in Holtfreter's solution (15 mM NaCl, 0.2 mM KCl, 0.6 mM NaHCO<sub>3</sub>, 0.2 mM MgSO<sub>4</sub>·7H<sub>2</sub>O, and 0.2 mM CaCl<sub>2</sub>) in 150-mm disposable Petri dishes at 24 °C and fed with rolled oats (Quaker Oats). Under these conditions, *E. japonensis* grows continuously to approximately 10 mm in length and reproduces asexually by fragmentation approximately every 2 weeks. Artificial amputation of *E. japonensis* was performed using needle-sharp tweezers (Feather, K-715). The amputees were cultured on filter paper (Whatman No 3030917) and kept moist at 24 °C with Milli-Q water in 60 × 10 mm disposable Petri dishes. *E. japonensis* was provided by Dr. Yoshida-Noro, C. (Nihon University, Tokyo, Japan).

Nieuwkoop and Faber stage<sup>66</sup> 51–53 Tadpoles (*X. laevis*) were purchased from a Japanese company (Watanabe Zoushoku). The tadpoles were maintained in tap water, which was left in a bucket overnight and filtered with canister filters (EHEIM Classic Model 2213). The tadpoles were fed with dumplings made of barely grass powder (Yamamoto Kampo Pharmaceutical Co.) and Ceramicon (Cera Japan Co.) mixed with Milli-Q water. The water and dumplings were replaced every day. Tail

amputation was performed using fine razor blades after the tadpoles were anesthetized with ice. The amputated tadpoles were kept in the water at 20 °C and allowed to regenerate. The regenerating tail tissues including the blastema (about 5 mm long from the amputation site) were collected. These experiments were performed by following the recommendations of the Guidelines for Proper Conduct of Animal Experiments of the Science Council of Japan. The protocol was approved by the Committee on the Ethics of Animal Experiments of Teikyo University.

### cDNA cloning and RNA probe preparation

Worms were cut into several fragments (normally 6–8) and allowed to regenerate for 24 h. Total RNA was extracted from approximately 100 regenerating fragments using TRIzol Reagent (Invitrogen) and reverse-transcribed using the SuperScript III kit (Invitrogen) using an oligo (dT) primer, by following the manufacturer's protocol. RT-PCR was performed using the following gene-specific primer pairs:

*soxC*: (Forward) 5'-ATGATACTAAGTTCTAAAAT-3' and (Reverse) 5'-TTAGTTCACCAATCTCTTA-3';  
*mmpReg*: (Forward) 5'-AACCAGTAACCAAGGCAACG-3' and (Reverse) 5'-CCCTCATGATTACGCCACT-3';  
*Ej-vasaI*: (Forward) 5'-GCCCCGTTGATCCTGATAAGA-3' and (Reverse) 5'-TGTTACCACATCGCCCTGTA-3';  
*Ej-vasa2*: (Forward) 5'-CTGGTAAACGGCATCATTCTC-3' and (Reverse) 5'-TTCTCAGCCACTCCGGCAC-3';  
*Ej-nanos*: (Forward) 5'-GCTCGTTGGAATCGATTAGTG-3' and (Reverse) 5'-CCCACACTGACTTGTGGTTG-3';

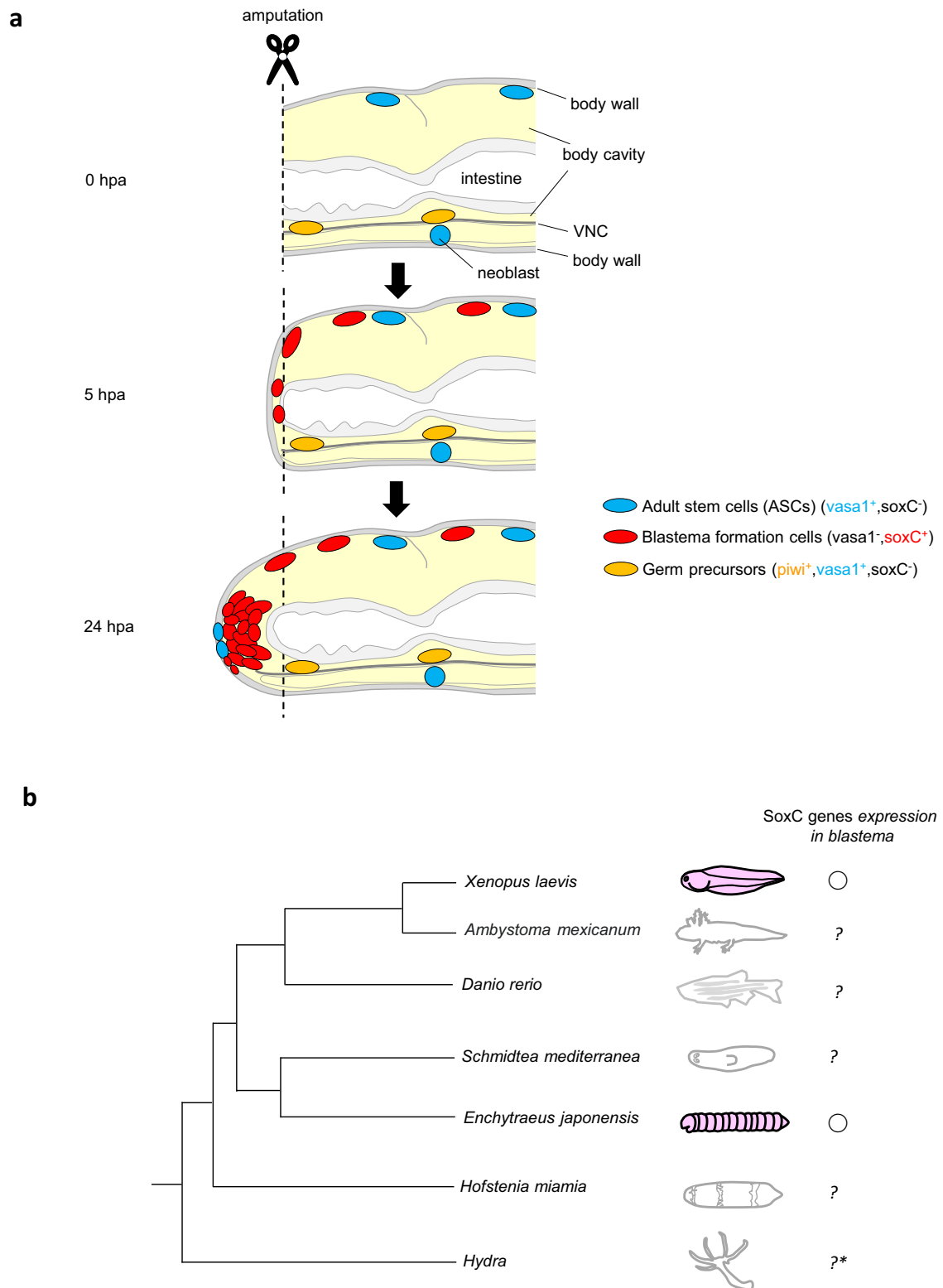


**Fig. 10 | Model for blastema formation in *E. japonensis*.** **a** GMP gene(s)-expressing cells (ASCs, shown in blue) are present in intact worms. *soxC*-expressing cells (shown in red) might be the cells supplied to the amputation site. The relationship between *soxC*-expressing cells and ASCs remains unclear. *soxC*-expressing cells were distinct from the population of cells on the VNC (shown in orange), which are

*Ej-piwi*-positive cells that serve as germ cell precursors. **b** Similarity in expression dynamics of SoxC genes in *E. japonensis* and *X. laevis* raised the possibility of the common cellular mechanisms underlying blastema formation in both species. In the cnidarian polyp *Hydra vulgaris*, *HvSoxC* was expressed in a transition state between i-cells and differentiated cells<sup>63</sup> (\*).

*Ej-pl10*: (Forward) 5'-TTCTGGCTGTGGGAAGAGTT-3' and (Reverse) 5'-CTGCTCCTCGAGCCATTTAG-3';

*Ej-piwi*: (Forward) 5'-GATCAAAACAGCACACGGATG-3' and (Reverse) 5'-CTTGGTCCCATCTTCTCTCG-3'.

The PCR products were subcloned into the pGEM-T easy vector (Promega), and the sequences were confirmed using Sanger sequencing. The plasmids containing the cDNA fragments for *soxC*, *mmpReg*, *Ej-vasa1*, *Ej-vasa2*, *Ej-nanos*, *Ej-pl10*, and *Ej-piwi*

were amplified using PCR with the M13 primer pair. The amplicons containing the T7 and SP6 promoter sites were purified using a PCR purification kit (Qiagen). Digoxigenin (DIG)-labeled sense and antisense RNA probes were prepared via in vitro transcription using the DIG RNA labeling kit (Roche). For double ISH analysis, *Ej-vasa1* fluorescein-labeled sense and antisense RNA probes were prepared through in vitro transcription using the fluorescein RNA labeling kit (Roche). For the preparation of *Xl-sox45* and *Xl-sox115* RNA probes, template DNA corresponding to full-length *Xl-sox45* (GenBank accession number: AF186844) or *Xl-sox115* (GenBank accession number: D83650) cDNA with T7 and SP6 promoter sites were synthesized and purchased from Twist Biosciences (South San Francisco, CA, USA).

## ISH

The worms were fixed overnight in 4% paraformaldehyde in 0.1 M phosphate-buffered saline (pH 7.5, PFA–PBS) at 4 °C. For cryoprotection, the fixed samples were placed overnight in an 18% sucrose/PFA–PBS solution at 4 °C. Subsequently, the worms with sucrose substitution were embedded in Tissue-Tek OCT compound (Sakura Finetech) using a Cryomold (Sakura Finetech), frozen immediately on dry ice, and stored at –80 °C until sectioning was performed. The frozen worm blocks were cut into 12 µm-thick sections using a cryostat (CM3050S; Leica Biosystems). Ten serial sections were mounted on a glass slide, and the sectioned specimens were fixed in PFA–PBS. After incubation in 10 µg/ml of proteinase K in 10 mM Tris/HCl and 1 mM EDTA, the specimens were post-fixed for 10 min in PFA–PBS, treated with 0.2 M HCl for 10 min, washed in PBS, and treated with 0.25% acetic anhydride in 0.1 M triethanolamine (pH 7.5) for 1 h. Hybridization was performed at 70 °C for 16 h in ULTRAhybTM Hybridization Buffer (Ambion) containing 500 ng/ml of the probe. The hybridized specimens were washed twice in wash buffer (50% formamide, 2× saline-sodium citrate (SSC) buffer) at 70 °C for 10 min, subjected to RNase treatment (20 mg/ml) in TNE (10 mM Tris, 1 mM EDTA, and 0.5 M NaCl [pH 7.5]) for 10 min, and washed in TNE for 10 min. After stringent washes with a series of SSC buffers, the specimens were incubated at 25 °C for 1 h in 1.5% blocking reagent (Roche, cat. # 11096176001) in DIG buffer I (100 mM Tris, 150 mM NaCl, pH 7.5), followed by incubation at 25 °C for 30 min with the alkaline phosphatase (AP)-conjugated anti-DIG antibody (Roche, cat. # 11093274910, 1:1000 dilution) in 1.5 % blocking reagents. After incubation, the specimens were washed twice at 25 °C with DIG buffer I for 20 min each time. For signal visualization, a chromogenic reaction was performed with a nitro blue tetrazolium/5-bromo-4-chloro-3-indolyl phosphate (NBT/BCIP, Roche) at 25 °C for 18 h until the signal pattern levelled off. The sections were counterstained with nuclear fast red solution (ScyTek Laboratorie). Bright-field images of whole sections on each slide glass were semi-automatically captured using the NanoZoomer 2.0HT or NanoZoomer XR systems (Hamamatsu Photonics). The microscopic fields of interest were cropped using the NDP.view2 software (ver. 2.7.25; Hamamatsu Photonics). The cropped images were converted to 8-bit images, and their brightness and contrast were adjusted using ImageJ (ver. 1.52a; National Institutes of Health). Sense probes were used as negative controls.

ISH was performed in the regenerating tadpole tail tissues using the same protocol as that used for worms with minor modifications. The frozen blocks were cut into 10 µm-thick sections using a cryostat. Six serial sections were mounted alternatively on two glass slides. One slide glass was used for the antisense probe and the other was used for the sense probe.

## Double ISH

The process from the re-fixation of sections to the chromogenic reaction with NBT/BCIP was performed as described earlier, except for hybridization. DIG-labeled RNA probes and fluorescein-labeled RNA probes were mixed and mounted simultaneously during hybridization. After the

first chromogenic reaction with NBT/BCIP, the AP-conjugated anti-DIG antibody was detached using 100 mM glycine (pH 2.2). After washing in PBS, the fluorescein-labeled probes were immunohistochemically detected using the AP-conjugated anti-fluorescein antibody (Roche, cat. # 11426338910, 1:1000 dilution). To visualize the signals, the second color chromogenic reactions were performed for 4 days at room temperature with SIGMAFAST Fast Red TR/Naphthol AS-MX tablets (Sigma-Aldrich, cat. # F4523). Sense probes were used as negative controls.

## Transcriptome seq, assembly, and annotation

Total RNA was extracted from the intact group (20 worms), blastema-poor group (about 100 fragments, 24 hpa) and blastema-rich group (about 100 fragments, 24 hpa) using TRIzol. Total RNA was further purified using RNeasy Plus Mini Kit (Qiagen) and submitted to Macrogen Corp. (<https://www.macrogen-japan.co.jp/>). The RNAs were purified by ribo-zero RNA removal kit (Illumina). Sequencing libraries were generated using the TruSeq Stranded mRNA LT Sample Prep Kit (Illumina). The libraries were sequenced on the NovaSeq 6000 platform, and 150 bp paired-end reads were generated. Raw sequences were deposited in the NCBI Short Read Archive (SRA) database (<http://www.ncbi.nlm.nih.gov/Traces/sra/>) under the accession numbers: SRR21413950, SRR21413951, and SRR21413952. Trimmomatic 0.38 (<http://www.usadellab.org/cms/?page=trimmomatic>) was used to quality trim the reads using the default settings, and the remaining clean reads were assembled using Trinity version trinityrnaseq\_r20140717, bowtie 1.1.2 (<https://github.com/trinityrnaseq/trinityrnaseq/wiki>) for transcriptome assembly without a reference genome. The longest transcript for each gene was selected as the unigene. For annotation analysis, the unigenes were searched against the KEGG, NCBI Nucleotide (NT), Pfam, Gene ontology (GO), NCBI non-redundant Protein (NR), UniProt, and EggNOG using BLASTN of NCBI BLAST version 2.9.0 (<https://blast.ncbi.nlm.nih.gov/Blast.cgi>) and BLASTX of DIAMOND version 0.9.21 (<https://github.com/bbuchfink/diamond>) software with an E-value default cut-off of 1.0E-5. The differentially expressed genes (DEGs) between the control (intact group) and regeneration groups (blastema-rich group or blastema-poor group) were identified using DEGseq analysis from the adjusted read count data. Statistical analyses were performed using fold change and Fisher's exact test using edgeR per comparison pair. The significant DEGs were determined by setting the threshold of fold change to >2 and Fisher's exact test at a raw p-value to <0.05. The unigenes were annotated based on BLASTX results, and the best alignments were used for downstream analyses. The GO and KEGG databases were used to predict the functions of the unigenes. Pathway analysis was performed using the KEGG Mapper tool ([http://www.genome.jp/kegg/tool/map\\_pathway2.html](http://www.genome.jp/kegg/tool/map_pathway2.html)). NCBI-gi numbers were applied as queries, and the acquired pathway search results were grouped under the KEGG pathway maps.

## 5'-rapid amplification of cDNA end (RACE) for *mmpReg*

5'-RACE was performed using the SMARTerRACE5'/3' kit (Takara Bio) according to the manufacturer's protocol. Briefly, after first-strand cDNA synthesis, PCR was performed using the gene-specific primer 5'-TCACCTCTCGACCTTCTCCTGG -3' and the universal primer included in the kit. Nested PCR was performed using the gene-specific primer 5'-CGGTACCCGGGGATCGCCATCCTGATGATAGCCTGATGAG -3' and the universal primer short included in the kit. The gene-specific primer for nested PCR contained a sequence at its 5' ends for cloning of RACE products (CGGTACCCGGGGATC). Cloning was performed using the In-Fusion Snap Assembly Master Mix (Takara Bio) according to the manufacturer's protocol.

## Phylogenetic analysis

Multiple sequence analysis was performed using Clustal X 2.1 [<https://clustalx.software.informer.com/2.1/>] using complete sequences from the selected eukaryotic species. A phylogenetic tree was constructed

using the Draw tree option in Clustal X<sup>67</sup> using the Neighbor-Joining algorithm with default settings (Gap opening:10, Gap extension:0.2, bootstrap number:1000), and the output file was analyzed using NJplot software<sup>68</sup> [<http://pbil.univ-lyon1.fr/software/njplot.html>]. The names of the genes and their accession numbers used for the phylogenetic analysis are listed in Supplementary Data 4. The *E. japonensis* sequences have been submitted to the DNA Data Bank of Japan (DDBJ) nucleotide database (LC727633, *Ej-mmpReg*; LC727634, *Ej-nanos*; LC727635, *Ej-piwi*; LC727636, *Ej-pll10*; LC727637, *Ej-soxC*; LC727638, *Ej-vasa1*; LC727639, *Ej-vasa2*; LC727632, *Ej-gapdh*).

### RNAi and inhibitor experiments

dsRNA was synthesized by following the protocol for RNAi in planarians with some modifications<sup>69</sup>. Briefly, DNA templates used for subsequent dsRNA synthesis were generated using PCR, and primers were designed to amplify limited regions of the cDNA sequence for each gene. Each primer contained a T7 promoter sequence at its 5'-end (TAATACGACTCACTATAGGGAGACCAC). The following PCR primers were used:

*soxC*: (Forward) 5'-TAAGCTGTGATGAGCTGAATCA-3' and (Reverse) 5'-CACCAATCTCTTAATATCCCA-3';

*mmpReg*: (Forward) 5'-AACCAGTAACCAAGGCAACG-3' and (Reverse) 5'-CCCTCATGATTTACGCCACT-3';

*GFP*: (Forward) 5'-GTGCCCATCTGGTGCAGCT-3' and (Reverse) 5'-ACTTGTACAGCTCGTCCATGCC-3'.

dsRNA was synthesized using the MegaScript<sup>TM</sup> T7 kit (Invitrogen) by following the manufacturer's instructions. The typical yield was approximately 50 µg of dsRNA per reaction. dsRNA (50 µg/100 µl) was diluted with 900 µl of Milli-Q water (5 µg/µl). Each worm was soaked in 5 µl of dsRNA in a 96-well plate at 24 °C. In all cases, the animals were transferred to a large volume of Milli-Q water and amputated 1 day after RNAi soaking. The amputated worms were allowed to undergo regeneration on filter paper that was kept moist with Milli-Q water. For the inhibitor experiment, MMP-2/MMP-9 inhibitor I (Cayman, CAS#193807-58-8) was used. The animals were soaked in 10 µM of inhibitor in 0.3% DMSO/PBS for 24 h at 24 °C, followed by amputation. The amputees were cultured on filter paper kept moist with 10 µM of inhibitor in 0.3% DMSO/PBS in Petri dishes at 24 °C.

### Determination of amputation site

The amputation site was determined on the image at a site where the curvature of the body wall suddenly changes. Care was taken to avoid chloragocytes and intestines as much as possible from the amputation site to the tip (Supplementary Fig. 13).

### Image analysis for evaluation of RNAi and inhibitor phenotype

The worms were fixed after 6 h or 24 h of amputation, and serial sections were subjected to ISH for *soxC*. We selected adjacent serial sections (three consecutive sections) in which signals were detected. The images, including blastema, were cropped and converted to 8-bit images using ImageJ software. The threshold for binarization was determined to appropriately measure the area of positive signals detected. The total area was calculated from the sum of the values obtained from three consecutive sections.

### Fluorescent image acquisition and quantification

For EdU labeling, the Click-iT EdU Alexa Fluor 488 Imaging Kit (Life Technologies, cat. # C10337) was used by following the manufacturer's protocol with minor modifications. Briefly, the amputated worms were allowed to regenerate for 3, 5, 8 or 24 h. The worms were exposed to EdU at a final concentration of 250 µM for the last 2 or 3 h. Then, the animals were fixed with PFA-PBS and incubated for 30 min in a freshly prepared EdU click-iT reaction cocktail. The nuclei were stained with DAPI (1/1000). The specimens were rinsed with PBS containing 0.1%

Tween 20 several times and mounted on slide glasses with 90% glycerol/PBS. Imaging was performed using CellVoyager CQ1 (Yokogawa). Z-stack images were acquired at approximately 5-µm intervals (15 sections). The area containing the blastema was enclosed manually. The total number of EdU-incorporated cells or DAPI-labelled cells was measured using the Cell Pathfinder software (Yokogawa) according to the manufacturer's protocol.

### RT and qRT-PCR analysis

The worms were cut into several fragments (normally 6–8) and allowed to regenerate for different times for experiments. Total RNA was extracted from each pool of fragments (approximately 200 fragments) using TRIzol, and cDNA was synthesized from 1 µg of total RNA using a Reverse-Transcription Kit (ThermoFisher). Quantitation of each gene product was performed using a LightCycler 96 System (Roche). Each reaction contained TB Green<sup>®</sup> Premix Ex Taq<sup>TM</sup> II (Qiagen), gene-specific primers, and the cDNA template and was subjected to PCR as follows: 95 °C for 30 s; 40 cycles of 95 °C for 5 s, 60 °C for 20 s; and 1 cycle at 65 °C for 15 s. The measurements were normalized to the expression level of *Ej-gapdh*. The mean of three replicate qRT-PCR assays was used for quantification. The following PCR primer pairs were used:

*soxC*: (Forward) 5'-TGCCAGCTTCTACCCTGAAGA-3' and (Reverse) 5'-GGTGCATGGTGCCAAACTT-3';

*mmpReg*: (Forward) 5'-CGATGGGCCAGGTATGGTACT-3' and (Reverse) 5'-ATGTCACCTCCTCGACCTTCTC-3';

*Ej-gapdh*: (Forward) 5'-AGGATTGGAGAGGAGGCAGAA-3' and (Reverse) 5'-CCGGTGGAGGATGGAATG-3'.

The tips of the tails were amputated from the tadpoles at st. 51–53 and allowed to regenerate for 0, 6, 24, and 48 h. The regenerating tail tissues including the blastema (about 5 mm long from the amputation site) were collected and pooled. Total RNA was extracted from each pool consisting of approximately 50 regenerating tail tissues. The measurements were normalized to the expression level of *Xl-elf1a*. The mean of four replicates was used for quantification. The following PCR primer pairs were used:

*Xl-sox4*: (Forward) 5'-CATCAAGCGGCCAATGAAC-3' and (Reverse) 5'-TGATTTTCTCCGCTCGATCT-3';

*Xl-sox11*: (Forward) 5'-GGGCTCCCACTTCGACTTC-3' and (Reverse) 5'-TGCGATCATCTCGCTGAGTT-3';

*Xl-elf1a*: (Forward) 5'-GGAACGGTGACAACATGC-3' and (Reverse) 5'-AGGCAGACGGAGAGGCTTA-3'.

### Statistical analysis

Sample size (n) is indicated in the figure legends. Statistical analyses were performed using EZR software based on R (version 2.7.1) or R (version 4.1.2). The methods used for each analysis are presented in the corresponding sections. All tests performed were two-sided.

### Reporting summary

Further information on research design is available in the Nature Portfolio Reporting Summary linked to this article.

### Data availability

Source data for graphs are provided with this paper. The raw sequences generated in this study were deposited in the NCBI Short Read Archive (SRA) database [<http://www.ncbi.nlm.nih.gov/Traces/sra/>] under the accession numbers: SRR21413950, SRR21413951, and SRR21413952. DNA sequences used for PCR in this study were deposited in the DNA Data Bank of Japan (DDBJ) nucleotide database under the accession numbers: *Ej-mmpReg*, LC727633; *Ej-nanos*, LC727634; *Ej-piwi*, LC727635; *Ej-pll10*, LC727636; *Ej-soxC*, LC727637; *Ej-vasa1*, LC727638; *Ej-vasa2*, LC727639; *Ej-gapdh*, LC727632. Source data are provided with this paper.



## References

- Barresi, M. & Gilbert, S. *Developmental Biology*. (Oxford University Press 2019).
- Morgan, T. H. Regeneration and Liability to Injury. *Science* **14**, 235–248 (1901).
- Sanchez Alvarado, A. Regeneration in the metazoans: why does it happen? *Bioessays* **22**, 578–590 (2000).
- Randolph, H. The regeneration of the tail in *Lumbriculus*. *J. Morphol.* **7**, 317–344 (1892).
- Tanaka, E. M. & Reddien, P. W. The cellular basis for animal regeneration. *Dev. Cell* **21**, 172–185 (2011).
- Tsonis, P. A. Regeneration in vertebrates. *Dev. Biol.* **221**, 273–284 (2000).
- Srivastava, M. Beyond Casual Resemblance: Rigorous Frameworks for Comparing Regeneration Across Species. *Annu Rev. Cell Dev. Biol.* **37**, 415–440 (2021).
- Bely, A. E. & Nyberg, K. G. Evolution of animal regeneration: re-emergence of a field. *Trends Ecol. Evol.* **25**, 161–170 (2010).
- Tornini, V. A. & Poss, K. D. Keeping at arm's length during regeneration. *Dev. Cell* **29**, 139–145 (2014).
- Currie, J. D. et al. Live Imaging of Axolotl Digit Regeneration Reveals Spatiotemporal Choreography of Diverse Connective Tissue Progenitor Pools. *Dev. Cell* **39**, 411–423 (2016).
- Bassat, E. & Tanaka, E. M. The cellular and signaling dynamics of salamander limb regeneration. *Curr. Opin. Cell Biol.* **73**, 117–123 (2021).
- Reddien, P. W. The Cellular and Molecular Basis for Planarian Regeneration. *Cell* **175**, 327–345 (2018).
- Ozpolat, B. D. & Bely, A. E. Developmental and molecular biology of annelid regeneration: a comparative review of recent studies. *Curr. Opin. Genet. Dev.* **40**, 144–153 (2016).
- Srivastava, M., Mazza-Curll, K. L., van Wolfswinkel, J. C. & Reddien, P. W. Whole-body acoel regeneration is controlled by Wnt and Bmp-Admp signaling. *Curr. Biol.* **24**, 1107–1113 (2014).
- Vogg, M. C., Galliot, B. & Tsiairis, C. D. Model systems for regeneration: Hydra. *Development* **146**, dev177212 (2019).
- Funayama, N. The cellular and molecular bases of the sponge stem cell systems underlying reproduction, homeostasis and regeneration. *Int J. Dev. Biol.* **62**, 513–525 (2018).
- Guedelhoefer, O. C. & Sanchez Alvarado, A. Planarian immobilization, partial irradiation, and tissue transplantation. *J. Vis. Exp.* **6**, 4015 (2012).
- Salo, E. & Baguna, J. Cell movement in intact and regenerating planarians. Quantitation using chromosomal, nuclear and cytoplasmic markers. *J. Embryol. Exp. Morphol.* **89**, 57–70 (1985).
- Lapan, S. W. & Reddien, P. W. *dlx* and *sp6-9* Control optic cup regeneration in a prototypic eye. *PLoS Genet* **7**, e1002226 (2011).
- Abnave, P. et al. Epithelial-mesenchymal transition transcription factors control pluripotent adult stem cell migration in vivo in planarians. *Development* **144**, 3440–3453 (2017).
- Seaver, E. C. Annelid models I: Capitella teleta. *Curr. Opin. Genet. Dev.* **39**, 35–41 (2016).
- Herlant-Mewis, H. Regeneration in annelids. *Adv. Morphog.* **4**, 155–215 (1964).
- Cornec, J.-P., Cresp, J., Delye, P., Hoarau, F. & Reynaud, G. Tissue responses and organogenesis during regeneration in the oligochaete *Limnodrilus hoffmeisteri* (Clap.). *Can. J. Zool.* **65**, 403–414 (1986).
- Stephan-Dubois, F. Migration and Differentiation of Neoblasts in Anterior Regeneration of *Lumbriculus variegatus* (Annelida, Oligochaeta). *C. R. Seances Soc. Biol. Fil.* **150**, 1239–1242 (1956).
- Wagner, D. E., Wang, I. E. & Reddien, P. W. Clonogenic neoblasts are pluripotent adult stem cells that underlie planarian regeneration. *Science* **332**, 811–816 (2011).
- Hill, S. D. Origin of the regeneration blastema in polychaete annelids. *Am. Zool.* **10**, 101–112 (1970).
- Martinez Acosta, V. G., Arellano-Carbajal, F., Gillen, K., Treeten, K. A. & Zattara, E. E. It Cuts Both Ways: An Annelid Model System for the Study of Regeneration in the Laboratory and in the Classroom. *Front Cell Dev. Biol.* **9**, 780422 (2021).
- Tadokoro, R., Sugio, M., Kutsuna, J., Tochinali, S. & Takahashi, Y. Early segregation of germ and somatic lineages during gonadal regeneration in the annelid *Enchytraeus japonensis*. *Curr. Biol.* **16**, 1012–1017 (2006).
- Myohara, M., Niva, C. C. & Lee, J. M. Molecular approach to annelid regeneration: cDNA subtraction cloning reveals various novel genes that are upregulated during the large-scale regeneration of the oligochaete, *Enchytraeus japonensis*. *Dev. Dyn.* **235**, 2051–2070 (2006).
- Bhambri, A. et al. Large scale changes in the transcriptome of *Eisenia fetida* during regeneration. *PLoS One* **13**, e0204234 (2018).
- Shao, Y. et al. Genome and single-cell RNA-sequencing of the earthworm *Eisenia andrei* identifies cellular mechanisms underlying regeneration. *Nat. Commun.* **11**, 2656 (2020).
- Cho, S. J. et al. Gene expression profile in the anterior regeneration of the earthworm using expressed sequence tags. *Biosci. Biotechnol. Biochem.* **73**, 29–34 (2009).
- Takeo, M., Yoshida-Noro, C. & Tochinali, S. Functional analysis of grimp, a novel gene required for mesodermal cell proliferation at an initial stage of regeneration in *Enchytraeus japonensis* (Enchytraeidae, Oligochaeta). *Int J. Dev. Biol.* **54**, 151–160 (2010).
- Nakamura, Y. A new fragmenting enchytraeid species, *Enchytraeus japonensis* from a cropped Kuroboku soil in Fukushima, Northern Japan (enchytraeids in Japan 5). *Edaphologia* **50**, 37–39 (1993).
- Myohara, M., Yoshida-Noro, C., Kobari, F. & Tochinali, S. Fragmenting oligochaete *Enchytraeus japonensis*: a new material for regeneration study. *Dev. Growth Differ.* **41**, 549–555 (1999).
- Yoshida-Noro, C. & Tochinali, S. Stem cell system in asexual and sexual reproduction of *Enchytraeus japonensis* (Oligochaeta, Annelida). *Dev. Growth Differ.* **52**, 43–55 (2010).
- Goldman, J. A. & Poss, K. D. Gene regulatory programmes of tissue regeneration. *Nat. Rev. Genet.* **21**, 511–525 (2020).
- Sarkar, A. & Hochedlinger, K. The sox family of transcription factors: versatile regulators of stem and progenitor cell fate. *Cell Stem Cell* **12**, 15–30 (2013).
- Bretscher, M. S. On the shape of migrating cells—a ‘front-to-back’ model. *J. Cell Sci.* **121**, 2625–2628 (2008).
- Zattara, E. E., Turlington, K. W. & Bely, A. E. Long-term time-lapse live imaging reveals extensive cell migration during annelid regeneration. *BMC Dev. Biol.* **16**, 6 (2016).
- Okuda, S. et al. KEGG Atlas mapping for global analysis of metabolic pathways. *Nucleic Acids Res* **36**, W423–W426 (2008).
- Bonnans, C., Chou, J. & Werb, Z. Remodelling the extracellular matrix in development and disease. *Nat. Rev. Mol. Cell Biol.* **15**, 786–801 (2014).
- Juliano, C. E., Swartz, S. Z. & Wessel, G. M. A conserved germline multipotency program. *Development* **137**, 4113–4126 (2010).
- Sugio, M. et al. Exploration of embryonic origins of germline stem cells and neoblasts in *Enchytraeus japonensis* (Oligochaeta, Annelida). *Gene Expr. Patterns* **8**, 227–236 (2008).
- Sugio, M., Yoshida-Noro, C., Ozawa, K. & Tochinali, S. Stem cells in asexual reproduction of *Enchytraeus japonensis* (Oligochaeta, Annelida): proliferation and migration of neoblasts. *Dev. Growth Differ.* **54**, 439–450 (2012).
- de Jong, D. M. & Seaver, E. C. Investigation into the cellular origins of posterior regeneration in the annelid *Capitella teleta*. *Regenerat. (Oxf.)* **5**, 61–77 (2018).
- Kozin, V. V. & Kostyuchenko, R. P. Vasa, PL10, and Piwi gene expression during caudal regeneration of the polychaete annelid *Alitta virens*. *Dev. Genes Evol.* **225**, 129–138 (2015).

48. Ozpolat, B. D. & Bely, A. E. Gonad establishment during asexual reproduction in the annelid *Pristina leidyi*. *Dev. Biol.* **405**, 123–136 (2015).
49. Heenan, P., Zondag, L. & Wilson, M. J. Evolution of the Sox gene family within the chordate phylum. *Gene* **575**, 385–392 (2016).
50. Angelozzi, M. & Lefebvre, V. SOXopathies: Growing Family of Developmental Disorders Due to SOX Mutations. *Trends Genet.* **35**, 658–671 (2019).
51. Tsujioka, H., Kunieda, T., Katou, Y., Shirahige, K. & Kubo, T. Unique gene expression profile of the proliferating *Xenopus* tadpole tail blastema cells deciphered by RNA-sequencing analysis. *PLoS One* **10**, e0111655 (2015).
52. Lai, A. G. & Aboobaker, A. A. EvoRegen in animals: Time to uncover deep conservation or convergence of adult stem cell evolution and regenerative processes. *Dev. Biol.* **433**, 118–131 (2018).
53. Reddien, P. W. et al. SMEDWI-2 is a PIWI-like protein that regulates planarian stem cells. *Science* **310**, 1327–1330 (2005).
54. Plickert, G., Frank, U. & Muller, W. A. Hydractinia, a pioneering model for stem cell biology and reprogramming somatic cells to pluripotency. *Int J. Dev. Biol.* **56**, 519–534 (2012).
55. Lim, R. S., Anand, A., Nishimiya-Fujisawa, C., Kobayashi, S. & Kai, T. Analysis of Hydra PIWI proteins and piRNAs uncover early evolutionary origins of the piRNA pathway. *Dev. Biol.* **386**, 237–251 (2014).
56. de Rosa, R., Prud'homme, B. & Balavoine, G. Caudal and even-skipped in the annelid *Platynereis dumerilii* and the ancestry of posterior growth. *Evol. Dev.* **7**, 574–587 (2005).
57. Zattara, E. E. & Bely, A. E. Evolution of a novel developmental trajectory: fission is distinct from regeneration in the annelid *Pristina leidyi*. *Evol. Dev.* **13**, 80–95 (2011).
58. Myohara, M. What role do annelid neoblasts play? A comparison of the regeneration patterns in a neoblast-bearing and a neoblast-lacking enchytraeid oligochaete. *PLoS One* **7**, e37319 (2012).
59. Gerber, T. et al. Single-cell analysis uncovers convergence of cell identities during axolotl limb regeneration. *Science* **362**, eaq0681 (2018).
60. Miao, Q. et al. SOX11 and SOX4 drive the reactivation of an embryonic gene program during murine wound repair. *Nat. Commun.* **10**, 4042 (2019).
61. Song, K. et al. Sox11b regulates the migration and fate determination of Muller glia-derived progenitors during retina regeneration in zebrafish. *Neural Regen. Res* **18**, 445–450 (2023).
62. Hoshiba, Y. et al. Sox11 Balances Dendritic Morphogenesis with Neuronal Migration in the Developing Cerebral Cortex. *J. Neurosci.* **36**, 5775–5784 (2016).
63. Siebert, S. et al. Stem cell differentiation trajectories in Hydra resolved at single-cell resolution. *Science* **365**, eaav9314 (2019).
64. Zeng, A. et al. Prospectively Isolated Tetraspanin(+) Neoblasts Are Adult Pluripotent Stem Cells Underlying Planaria Regeneration. *Cell* **173**, 1593–1608 e1520 (2018).
65. Hulett, R. E. et al. Acoel single-cell atlas reveals expression dynamics and heterogeneity of adult pluripotent stem cells. *Nat. Commun.* **14**, 2612 (2023).
66. Nieuwkoop D. P., Faber, J. *Normal Table of Xenopus laevis (Daudin): A Systematical and Chronological Survey of the Development from the Fertilized Egg Till the End of Metamorphosis*. Cold Spring Harbor Laboratory Press (1967).
67. Larkin, M. A. et al. Clustal W and Clustal X version 2.0. *Bioinformatics* **23**, 2947–2948 (2007).
68. Perriere, G. & Gouy, M. WWW-query: an on-line retrieval system for biological sequence banks. *Biochimie* **78**, 364–369 (1996).
69. Shibata, N. & Agata, K. RNA Interference in Planarians: Feeding and Injection of Synthetic dsRNA. *Methods Mol. Biol.* **1774**, 455–466 (2018).

## Acknowledgements

We thank Dr. Takahiro Ito, Dr. Shinji Takada, and Dr. Yusuke Mii for critically reading the manuscript. We thank Dr. Mii for providing protocols and apparatus for raising the tadpoles. We would like to thank Editage ([www.editage.com](http://www.editage.com)) for English language editing. This study was supported by a Teikyo University Research Encouragement Grant (T.F.), a Fund for the Promotion of Joint International Research (Fostering Joint International Research [B]) (T. F., K.J.H. 19KK0211), Grants-in-Aid for Scientific Research from the Japan Society for the Promotion of Science (S.Y., 24590096, 15K07945, 18K06667; N.A., 24790089, 20K06915; C.M., 20K16472; and K.J.H., 26440182, 17K07492, 20K06747), the Uehara Memorial Foundation (S.Y.), the Sagawa Foundation for Promotion of Cancer Research (S.Y.), and a Grant-in-Aid for Scientific Research on Innovative Areas Memory dynamism (26115522), Adaptive circuit shift (15H01449), and Evolving linguistics (20H05012) from the Ministry of Education, Culture, Sports, Science and Technology (K.J.H.), the Naito Foundation (K.J.H.), and the Japan Foundation for Applied Enzymology (K.J.H.).

## Author contributions

T.F. and S.Y. designed the study and performed the experiments; T.F., N.A., C.M., K.J.H., and S.Y. analyzed the data and wrote the paper. All authors have reviewed the manuscript.

## Competing interests

The authors declare no competing interests.

## Additional information

**Supplementary information** The online version contains supplementary material available at <https://doi.org/10.1038/s41467-024-50865-1>.

**Correspondence** and requests for materials should be addressed to Shinji Yamaguchi.

**Peer review information** *Nature Communications* thanks José Martín-Durán and the other, anonymous, reviewer(s) for their contribution to the peer review of this work. A peer review file is available.

**Reprints and permissions information** is available at <http://www.nature.com/reprints>

**Publisher's note** Springer Nature remains neutral with regard to jurisdictional claims in published maps and institutional affiliations.

**Open Access** This article is licensed under a Creative Commons Attribution-NonCommercial-NoDerivatives 4.0 International License, which permits any non-commercial use, sharing, distribution and reproduction in any medium or format, as long as you give appropriate credit to the original author(s) and the source, provide a link to the Creative Commons licence, and indicate if you modified the licensed material. You do not have permission under this licence to share adapted material derived from this article or parts of it. The images or other third party material in this article are included in the article's Creative Commons licence, unless indicated otherwise in a credit line to the material. If material is not included in the article's Creative Commons licence and your intended use is not permitted by statutory regulation or exceeds the permitted use, you will need to obtain permission directly from the copyright holder. To view a copy of this licence, visit <http://creativecommons.org/licenses/by-nc-nd/4.0/>.

© The Author(s) 2024